**A dual role for the class III PI3K, Vps34, in platelet production and thrombus growth**

Short title: Vps34 in platelet production and thrombus growth

Colin Valet[1*], Marie Levade[1,2*], Gaëtan Chicanne[1], Benoit Bilanges[3], Cendrine Cabou[1,4], Julien Viaud[1], Marie-Pierre Gratacap[1], Frédérique Gaits-Iacovoni[1], Bart Vanhaesebroeck[3], Bernard Payrastre[1,2$] and Sonia Severin[1$]

[1] *Inserm U1048 and Université Toulouse 3, I2MC, Toulouse, France*

[2] *CHU de Toulouse, Laboratoire d'Hématologie, Toulouse, France*

[3] *UCL Cancer Institute, Paul O'Gorman Building, University College London, 72 Huntley Street London WC1E 6DD, UK*

[4] *Faculté de Pharmacie, Chemin des maraichers, Toulouse, France*

[*] *These authors contribute equally to this work*

[$] *These authors share senior authorship*

**Address correspondence to:**

Sonia Severin, Inserm U1048 and Université Toulouse 3, I2MC, 31432 Toulouse Cedex 4, France. Phone: +33-531224143; Email: sonia.severin@inserm.fr

Scientific section heading: Platelets and Thrombopoiesis

Text word count : 4372
Abstract word count : 242
Number of figures : 6
Number of references : 46

**Key points**

- Vps34 controls intracellular trafficking, migration and platelet production in megakaryocytes.
- Vps34 and its stimulation-dependent PI3P production regulate platelet secretion and thrombus growth

## ABSTRACT

To uncover the role of Vps34, the sole class III phosphoinositide 3-kinase, in megakaryocytes (MKs) and platelets, we created a mouse model with Vps34 deletion in the MK/platelet lineage (*Pf4*-Cre/Vps34$^{lox/lox}$). Deletion of Vps34 in MKs led to the loss of its regulator protein Vps15, and was associated with microthrombocytopenia and platelet granule abnormalities. While Vps34 deficiency did not impact on MK polyploidisation or proplatelet formation, it dampened MK granule biogenesis and directional migration towards an SDF1α gradient, leading to ectopic platelet release within the bone marrow. In MKs, the level of phosphatidylinositol 3-monophosphate (PI3P) was significantly reduced by Vps34 deletion resulting in endocytic/trafficking defects. In platelets, the basal level of PI3P was only slightly affected by Vps34 loss while the stimulation-dependent pool of PI3P was significantly decreased. Accordingly, a significant increase in the specific activity of Vps34 lipid kinase was observed following acute platelet stimulation. Similar as in Vps34-deficient platelets, ex vivo treatment of WT mouse or human platelets with Vps34 specific inhibitors, SAR405 and VPS34-IN1, induced abnormal secretion and affected thrombus growth at arterial shear rate, indicating a role for Vps34 kinase activity in platelet activation, independently from its role in MKs. In vivo, Vps34 deficiency had no impact on tail bleeding time but significantly reduced platelet prothrombotic capacity following carotid injury. This study uncovers a dual role for Vps34 as a regulator of platelet production by MKs and as an unexpected regulator of platelet activation and arterial thrombus formation dynamics.

## INTRODUCTION

Phosphoinositide 3-kinases (PI3Ks) are important lipid kinases producing D3-phosphorylated phosphoinositides that organize functional protein complexes regulating various biological processes[1,2]. The sole class III PI3K, Vps34, represents the most ancient form of PI3Ks and was initially identified in yeast with an essential role in vacuolar homeostasis[3]. Vps34 occurs in complex with its regulatory protein kinase subunit, Vps15 and specifically catalyzes the conversion of phosphatidylinositol into phosphatidylinositol 3-monophosphate (PI3P). This lipid, present in relatively low amounts in cells, is known to play a central role in the regulation of intracellular trafficking[4]. In mammals, Vps34 has been shown to regulate endosomal trafficking, autophagosome formation and mTOR activation through PI3P production[5]. Recently, the organismal role of Vps34 has been investigated using mouse gene targeting strategies. Loss of the *Pik3c3* gene in mouse causes early embryonic lethality (between E7.5 and E8.5) due to severe decreased cell proliferation capacity[6]. In vivo studies using the tissue-specific cre-lox system have shown an important role for Vps34 in heart[7,8], liver[7], T cell[9], podocyte[10,11] and skeletal muscle[12] functions and in sensory, cortical and hippocampal neuron integrity[13,14] by regulating, through two different protein complexes, endosomal and/or the autophagic pathways.

At present, the role of Vps34 and its lipid product, PI3P, remains unknown in megakaryocytes (MKs) and platelets. Platelets are small anucleated blood cells playing a pivotal role in preventing excessive blood loss in response to vascular injury by adhering to exposed extracellular matrix and forming an haemostatic plug. Platelets are also strongly involved in atherothrombosis, a major cause of death worldwide, and are the target of anti-thrombotic drugs. To daily produce around $10^{11}$ platelets into the circulation, MKs migrate close to bone marrow sinusoids and protrude long cytoplasmic extensions called proplatelets into the sinusoidal lumen to release de novo circulating platelets[15]. In MKs and platelets, endocytosis

and intracellular trafficking are involved in secretory granule biogenesis as well as receptor and organelle trafficking[16-19].

The aim of this study was to define the role for the Vps34/PI3P axis in MK differentiation and platelet production and function. This is important to provide new insights into these complex mechanisms and also, because Vps34 inhibitors which may impact on haemostasis are under development to improve chemotherapy[20,21]. To tackle these questions we used both a genetic approach in mice and pharmacological inhibitors. We show that Vps34 has two important roles: i) for platelet production in MKs where it controls the production of an important pool of PI3P, regulates MK migration and the subsequent platelet release in the blood, and impacts on trafficking and granule biogenesis, and ii) for platelet functions where it controls the production of a stimulation-dependent pool of PI3P that modulates platelet secretion and thrombus growth under arterial shear stress. This study provides new insights into the importance of the Vps34/PI3P axis as a regulator of both platelet production by MKs and platelet activation during arterial thrombus growth.

## METHODS

**Animals:** 8 to 14 weeks-old C57BL/6 mice were used for all experiments and housed in the Anexplo (Toulouse) vivarium according to institutional guidelines. Ethical approval for animal experiments was obtained from the French Ministry of Research in agreement with European Union guidelines.

**Human blood samples:** Heparinized blood from healthy donors was purchased from the Etablissement Français du Sang (Toulouse) and immediately processed for experiments.

**In vitro PI3K activity assay and lipid analysis:** Vps34 immunoprecipitation and in vitro kinase assay were performed on washed platelets as previously described[22]. PI3P mass assay and phosphoinositide labeling were performed as previously described[23,24].

**Primary MK purification and culture, immunofluorescence and flow cytometry on mature MKs as well as electron microscopy on native bone marrow and proplatelet formation assay from bone marrow explants** are described in the supplemental Methods.

**MK migration assay:** Chemotaxis was assessed using a Dunn chamber (Chemotaxis Dunn, Hawksley). MKs were allowed to adhere onto fibronectin-coated coverslips (20 μg/mL) at 37°C for 1 h. The coverslip was then placed onto the Dunn chamber where the inner well was filled with serum-free medium and the outer well with serum-free medium containing 300 ng/mL of SDF1α. Videomicroscopy was performed for 6 h with an Axio Observer.Z1 inverted microscope operated with Zen software (Carl Zeiss) using an ORCA R2 camera (Hamamatsu, Japan) and a 10x, 0.30 EC Plan Neofluar objective lens. Migration analysis was performed using ImageJ and Chemotaxis tool plug-in.

**Bone marrow immunostaining:** Mouse femora were fixed with 4% paraformaldehyde and 5 mM sucrose and dehydrated using a graded sucrose series. Subsequently, the samples were

embedded in OCT matrix (CellPath) and shock-frozen in liquid nitrogen. Five-micrometre-thick cryosections were probed with rabbit anti-human vWF antibody to specifically label MKs/platelets and mouse/rat anti-mouse FABP4/A-FABP antibody to stain microvascular endothelial cells[25] followed by Alexa Fluor® secondary antibodies. Nuclei were stained using DAPI. Samples were visualized with a LSM780 operated with Zen software (Carl Zeiss) using a 63x, 1.4 NA Plan Apochromatic objective lens (Carl Zeiss). Image analysis was performed using ImageJ.

**Platelet lifespan, immune-induced thrombocytopenia, carotid artery thrombosis and tail bleeding time** are described in the supplemental Methods.

**Washed murine platelet preparation, flow cytometry, electron microscopy, aggregation, secretion, αIIbβ3 integrin function assays and thrombus formation assays on collagen** are described in the supplemental Methods.

**Statistical analysis:** Data are expressed as mean ± SEM. Significance of differences was determined using two-tailed Student's test, one-way ANOVA, two-way ANOVA or one sample *t* test. P values < 0.05 were considered significant (*p<0.05, **p<0.01, ***p<0.001).

## RESULTS

### Conditional genetic invalidation of Vps34 in the MK/platelet lineage

To generate a mouse model with conditional invalidation of Vps34 activity, exon 21 of the kinase domain of the *Pik3c3* gene was flanked with *LoxP* sites (*Pik3c3*$^{lox}$, B.B. and B.V., manuscript in preparation). Excision of exon 21 encoding the kinase domain of Vps34 specifically in the MK/platelet lineage was obtained by breeding *Pik3c3*$^{lox/lox}$ mice with *Pf4*-Cre transgenic mice to generate *Pf4*-Cre-*Pik3c3*$^{lox/lox}$ mice (referred to as Vps34 in the figures). Littermate *Pik3c3*$^{lox/lox}$ (referred to as WT) mice were used as controls. Platelet and MK lysates were analyzed by western blotting to assess the stability of the Vps34 protein lacking the exon 21 coding sequence. A dramatic reduction in Vps34 protein expression level was observed specifically in MKs (84.3% ± 2.6%) and platelets (87.8% ± 1.5%) from *Pf4*-Cre-*Pik3c3*$^{lox/lox}$ mice (Figure S1A and S1B). Similarly, the level of Vps15, a Vps34 regulatory and associated protein kinase, was also strongly decreased in MKs and platelets from *Pf4*-Cre-*Pik3c3*$^{lox/lox}$ mice (Figure S1A). This correlates with a previous study reporting the requirement of Vps34 to maintain the protein complex integrity[26]. Vps34 deletion had no impact on class I and II PI3K isoform expression in MKs and platelets (Figure S1A). Some residual lipid kinase activity (17.1% ± 4.1%) was detected in Vps34 immunoprecipitates from Vps34-deficient platelets (Figure S1C) suggesting efficient but incomplete Cre recombinase activity. *Pf4*-Cre-*Pik3c3*$^{lox/lox}$ mice are viable and fertile, develop normally with no apparent morphological abnormalities and showed no signs of spontaneous bleeding.

### Mild microthrombopenia and platelet granule abnormalities in the absence of Vps34

Deletion of Vps34 in the MK/platelet lineage resulted in a microthrombocytopenia of moderated intensity. As shown in Figure 1A, there was a significant reduction in the platelet count (22.4% ± 1.9 %, $p<0.001$) and in the mean platelet volume (6.18 $\mu m^3$ ± 0.24 $\mu m^3$ for

*Pf4*-Cre-*Pik3c3*$^{lox/lox}$ mice versus 7.39 μm$^3$ ± 0.22 μm$^3$ for WT mice, p<0.01; with a significant increase in mice with a mean platelet volume between 4 and 7 μm$^3$). Expression levels of major platelet surface receptors (α2β1, αIIbβ3, GPVI and functional GPIb-IX-V) were comparable in *Pf4*-Cre-*Pik3c3*$^{lox/lox}$ and WT platelets (Figure S1D and Videos 1 and 2).

Circulating platelet count and size are the net result of a balance between platelet production and clearance that can be evaluated by in vivo measurements of platelet count recovery after immune-induced depletion and platelet lifespan. As shown in Figure 1B and C, platelet lifespan was normal in *Pf4*-Cre-*Pik3c3*$^{lox/lox}$ mice whereas platelet production was altered. Despite a normal platelet recovery kinetic following anti-GPIbα antibody-induced thrombocytopenia, a reduced number of platelets was produced in *Pf4*-Cre-*Pik3c3*$^{lox/lox}$ mice (Figure 1C). Accordingly, serum TPO levels, which are classically inversely proportional to platelet count, were significantly elevated in *Pf4*-Cre-*Pik3c3*$^{lox/lox}$ (Figure 1C). However, increased TPO levels can also reflect abnormalities in clathrin-dependent endocytosis of its receptor, Mpl[19,27]. While total and surface expression of Mpl in resting WT and Vps34-deficient platelets were comparable (Figure S2A), we observed a significant decrease in Mpl endocytosis after 20 minutes of TPO stimulation in Vps34-deficient platelets (Figure 1C). This indicates that elevated serum TPO levels results from a decreased platelet count and a defective Mpl endocytosis in platelets from *Pf4*-Cre-*Pik3c3*$^{lox/lox}$ mice. Overall, these findings show that *Pf4*-Cre-*Pik3c3*$^{lox/lox}$ mice microthrombocytopenia is due to a defective platelet production by MKs.

Morphological analysis by transmission electron microscopy (TEM) revealed an abnormal granule distribution in Vps34-deficient platelets (Figure 1D). These platelets displayed a 33.2% ± 3.1% reduction in the number and a 44.5% ± 3.4% increase in the size of α-granules compared to WT (Figure 1D). Abnormalities of dense granules were also observed with a 44.8% ± 3.1% reduction in number compared to WT (Figure 1D). We also found that

fibrinogen internalization was significantly delayed in Vps34-deficient platelets (Figure S2B). Thus, the decreased efficiency of αIIbβ3/fibrinogen and Mpl/TPO endocytosis demonstrate an important contribution of Vps34 in clathrin-mediated endocytosis in platelets. Despite a delayed endocytosis in Vps34-deficient platelets, α- or dense- granule contents (von Willebrand factor (vWF), fibrinogen or serotonin) in Vps34-deficient platelets were similar to that of WT platelets (Figure S2C). Of note, platelet mitochondrial content and activity appeared normal in Vps34-deficient platelets (Figure S2D).

Overall, these data indicate that Vps34 specifically regulates platelet production, endocytosis and granule homeostasis.

**Vps34 is critical for MK migration and granule biogenesis**

To gain insight into the mechanisms leading to the observed platelet phenotype, we then analyzed MK morphology and functions. As shown in Figure 2A and Figure S3A-C, resident bone marrow MKs or bone marrow-derived MKs from *Pf4*-Cre-*Pik3c3*$^{lox/lox}$ mice displayed similar number, size, ploidy levels, demarcation membrane system and proplatelet-producing capacity compared to WT MKs. MK ploidy levels and proplatelet extension were also not affected following pharmacological inhibition of Vps34 using the specific Vps34 inhibitor, VPS34-IN1[20] (Figure S3B and S3C). However, transmission electron microscopy of MKs in their native bone marrow showed that Vps34-deficient MKs display less (21.4% ± 3.7% reduction in number) but bigger (26.5% ± 2.4% increase in size) α-granules compared to WT MKs (Figure 2A), indicating that platelet granule defects originate from an abnormal biogenesis in MKs.

An important stage of megakaryopoiesis prior to platelet release in the circulation is MK migration from the proliferative osteoblastic niche to the capillary-rich vascular niche in response to an SDF1α gradient[28]. We found that in vitro MK migration toward an SDF1α

gradient on fibronectin, a major extracellular matrix component of the bone marrow[29], was significantly affected when Vps34 is absent or inhibited. While the migration distance was comparable to WT MKs, deficiency or inhibition of Vps34 induced a significant reduction in megakaryocyte directionality towards SDF1α. The migration paths demonstrated that Vps34-deficient MKs moved over short distances before changing direction indicating a lack of directional persistence towards the SDF1α gradient (Figure 2B). Immunostaining of bone marrow sections of intact femora showed that Vps34-deficient MKs more frequently released platelets outside the sinusoids directly into the bone marrow compartment than WT MKs (Figure 2C). Altogether, these findings are consistent with a critical role for Vps34 in regulating directional MK migration and the subsequent platelet release into sinusoid vessels. This strongly suggests that thrombocytopenia in *Pf4*-Cre-*Pik3c3*$^{lox/lox}$ mice is caused by the inability of mature MKs to reach bone marrow sinusoids resulting in the observed ectopic platelet release.

**Vps34 deletion impacts on intracellular trafficking and PI3P production in MKs**

Both cell migration[30] and granule biogenesis[17,18] are regulated by intracellular trafficking mechanisms such as endocytosis, recycling and/or degradation. Besides normal transferrin receptor and αIIbβ3 integrin surface expression levels (Figure S3D), Vps34-deficient MKs displayed a significant reduction in transferrin and fibrinogen endocytosis after 20 min (Figure 3A and 3B). Moreover, large and less abundant fibrinogen-containing vesicles were observed over time by super resolution microscopy in Vps34-deficient MKs compared to WT MKs (Figure 3C). These data show the important role of Vps34 in clathrin mediated-endocytosis in MKs as observed for platelets (Figure 1C and S2B) and highlight its role in trafficking from the plasma membrane to granules in MKs. Consistent with these trafficking defects, we found by confocal microscopy a significant decreased number and increased size

of clathrin-positive vesicles as well as an accumulation of large early endosomes, as shown by an increased number (28.2% ± 2.7%) and size (16.7% ± 2.5%) of EEA1-positive vesicles in Vps34-deficient MKs (Figure 3D). Confocal analysis of LAMP1 and lysotracker labelling demonstrated a defect in early endosome to lysosome transition in Vps34-deficient MKs compared to WT MKs. In addition, Rab11 labeling demonstrated a decrease in the number (43.9% ± 4.4%) and size (22.5% ± 1.3%) of recycling endosomes in Vps34-deficient MKs (Figure 3E). This is consistent with elevated level of internalized transferrin at late time points (60 and 120 min) (Figure 3A) and point to an impaired endosomal recycling. Altogether, these data show the existence of a general trafficking defect in Vps34-deficient MKs. This defect was not due to a loss of clathrin, early endosomal Rab5, late endosomal Rab7 or recycling endosomal Rab 11 GTPases expression (Figure S3E). Interestingly, the level of Vps34 lipid product, PI3P, quantified by a specific mass assay[23] and confocal microscopy using a specific anti-PI3P antibody, showed a significant reduction in Vps34-deficient MKs (Figure 3F and G). This reduction (from 30 to 40% compared to WT MKs) demonstrates the significant contribution of Vps34 to the level of PI3P but also suggested the existence of other enzymatic sources of PI3P in MKs. Overall, these data indicate a role for Vps34 in PI3P production and in the regulation of the endocytic/endosomal pathway in MKs with consequences in fibrinogen trafficking and in turn granule biogenesis.

**In platelets, Vps34 is critical for the stimulation-dependent PI3P pool, but not for the basal PI3P pool**

We next analyzed the impact of Vps34 deletion or inhibition in platelets using our mouse model and the Vps34 specific inhibitors (VPS34-IN1 and SAR405)[20,21]. We first focused on the production of PI3P by using both a specific mass assay[23] quantifying the total PI3P amount and an HPLC analysis[24] following short term $^{32}$Pi-labelling to determine the acute

changes in phosphoinositides following platelet stimulation. In resting platelets, the level of PI3P was modestly decreased (10.1% ± 1.3%) when Vps34 was deficient or pharmacologically inhibited with VPS34-IN1 (Figure 4A). Surprisingly, following CRP or thrombin stimulation, the inducible pool of PI3P was clearly affected (Figure 4B). HPLC analysis confirmed these defective responses (Figure 4C). No significant difference was observed in the amount of other lipid messengers including phosphatidylinositol 3,4-bisphosphate ($PI(3,4)P_2$), phosphatidylinositol 3,4,5-trisphosphate ($PI(3,4,5)P_3$) and phosphatidic acid in resting or agonist-stimulated platelets (Figure S4). These data indicate that Vps34 is responsible for a small pool of basal PI3P in platelets and strongly involved in the agonist-dependent-pool of PI3P. To check whether Vps34 could be activated during platelet stimulation, we assayed its lipid kinase activity after immunoprecipitation. Acute WT platelet stimulations with thrombin or CRP resulted in a significant increase in Vps34 lipid kinase specific activity (Figure 4D). These data implicate a role for Vps34 activity in acute platelet stimulation.

**Vps34 kinase activity regulates thrombus growth**

We first tested the implication of Vps34 in platelet responses in vivo and found a normal tail bleeding time of *Pf4*-Cre-*Pik3c3*$^{lox/lox}$ mice (Figure 5A). The prothrombotic function of platelets tested after $FeCl_3$-induced mouse carotid injury was significantly decreased with nearly 50% of *Pf4*-Cre-*Pik3c3*$^{lox/lox}$ mice protected against occlusive arterial thrombus formation (Figure 5B).

Ex vivo thrombus formation assay performed under physiological arterial or arteriolar wall shear rates (500 and 1500 $s^{-1}$ respectively) using *Pf4*-Cre-*Pik3c3*$^{lox/lox}$ mice blood perfused over a collagen surface showed that Vps34-deficient platelets, despite their ability to normally attach to collagen fibres (Figure S5A), formed significantly smaller thrombi compared to WT

platelets (Figure 5C and D). When WT mice blood was treated ex vivo with Vps34 inhibitors and then perfused on a collagen matrix, thrombus formation was affected to a similar extent as for *Pf4*-Cre-*Pik3c3*$^{lox/lox}$ mice blood (Figure S5B). Importantly, when human blood was treated with Vps34 inhibitors, again a similar defect in thrombus growth was observed (Figure 5E). These data demonstrate that inhibition of Vps34 kinase activity in platelets, independently of its implication in MKs and platelet production, decreases platelet thrombus growth at arterial and arteriolar flow.

**Vps34 kinase activity is required for controlled platelet secretion**

To further analyze the thrombus formation defect, we performed aggregometry assays on platelets from *Pf4*-Cre-*Pik3c3*$^{lox/lox}$ mice and on human platelets treated with the Vps34 inhibitor. The mouse platelet aggregation responses to CRP, collagen, thrombin, thromboxane A2 analogue or ADP were not affected by Vps34 deficiency (Figure S6A). Platelet shape change and filopodia formation were also normal (Figure S6B) as well as thrombin or CRP-induced JON/A binding, reflecting normal αIIbβ3 integrin activation (Figure S6C). PI3P is known to contribute to the regulation of NADPH oxidase complex subunits[31], therefore we measured the production of reactive oxygen species in response to CRP or thrombin. This production was not affected in Vps34-deficient platelets nor was the thromboxane A2 production (Figure S6D and S6E), consistent with the fact that indomethacin treatment did not modify the thrombus growth difference between WT and *Pf4*-Cre-*Pik3c3*$^{lox/lox}$ mice blood (Figure S6F). Aggregation responses of human platelets were also not affected following pharmacological inhibition of Vps34 (Figure S6G).

Interestingly, in the absence of Vps34 and despite a normal amount of granule content (Figure S2C), dense granule release (assessed by ATP secretion; Figure 6A) as well as α-granule release (assessed by vWF secretion; Figure 6B) were significantly faster and exacerbated in

response to platelet acute stimulation. This increased secretion response was also observed after treatment of WT platelets with the Vps34 inhibitor (Figure 6C and D). Consistent with this, Vps34-deficient platelets displayed an enhanced spreading on fibrinogen that was fully counteracted by hydrolysis of secreted ATP/ADP by addition of apyrase (Figure 6E). Since a low solute transport is important to maintain elevated concentration of molecules secreted by platelets within the thrombus and to allow efficient thrombus growth[32,33], we checked whether the exacerbated secretion response could influence thrombus formation under arterial flow condition. Measurement of the serotonin level, in *Pf4*-Cre-*Pik3c3*$^{lox/lox}$ mice whole blood or WT mice whole blood treated with Vps34 inhibitor, recovered after perfusion on a collagen matrix showed an increased level of serotonin. This indicates that Vps34-deficient platelets or Vps34-inhibited WT platelets forming thrombi on collagen surface had an exacerbated secretion, resulting in higher level of secreted molecules in the circulation (Figure 6F). Accordingly, when $DiOC_6$-labelled whole blood from WT mice was perfused under physiological shear rate over preformed WT or *Pf4*-Cre-*Pik3c3*$^{lox/lox}$ thrombi, we observed that Vps34-deficient platelet thrombi were significantly less efficient to recruit WT circulating platelets to allow thrombus growth (Figure 6G).

Taken together, these data show that Vps34 kinase activity controls the intensity and timing of platelet secretion, which likely impacts on thrombus growth under arterial wall shear rate.

## DISCUSSION

By creating a mouse model of MK/platelet lineage-specific Vps34 deletion and using two unrelated Vps34 selective inhibitors, we revealed a dual role for Vps34 in MKs and in platelets. *Pf4*-Cre-*Pik3c3*$^{lox/lox}$ mice displayed a moderate microthrombocytopenia due to a platelet production defect rather than an abnormal platelet lifespan. While nuclear and membrane maturation as well as proplatelet extension were normal in MKs when Vps34 is absent or inhibited, directional MK migration towards a SDF1α gradient was strongly affected. In the bone marrow, MKs migrate from the osteoblastic niche to the vascular niche to deliver platelets in the blood flow. Most likely as a result of this directional migration defect, *Pf4*-Cre-*Pik3c3*$^{lox/lox}$ mice showed an increased presence of platelets in the bone marrow outside the sinusoidal vessels, consistent with the mild microthrombocytopenia observed in these mice. Of note, this is also the case of patients with Wiskott-Aldrich syndrome (WAS) and profilin 1-deficient mice where microthrombocytopenia has been reported to result from accelerated platelet turn-over and premature platelet release into the bone marrow associated to defective MK migration towards the SDF1α gradient[34,35]. Directed cell migration is a spatially organized process, governed by the cell ability to sense chemokine gradient and then transduce adequate signalling for the cell to polarize and move by chemotaxis that depends on intracellular trafficking of cell surface receptors[30]. SDF1α receptor-driven CXCR4 polarization has been shown to be important for MK directed migration towards an SDF1α gradient[36]. Thus, a defect that might explain the lack of directional migration of Vps34-deficient MKs is the herein documented defective trafficking (clathrin-mediated endocytosis and recycling) and the subsequent inadequate positioning of the SDF1α receptor, CXCR4, at the migration front. Unfortunately, the lack of efficient molecular tools to study CXCR4 in primary MKs did not allow us to evaluate this hypothesis. Impaired trafficking of other receptors, such as the fibronectin receptor α5β1 integrin since

migration was assayed on a fibronectin matrix, could take part into the lack of MK directionality and in turn cause ectopic platelet release within the bone marrow[37]. This study implements the short list of publications highlighting the important role of endocytosis in MKs and platelets[16,19]. For instance, deletion of dynamin 2, a major actor of clathrin-mediated endocytosis, in MKs and platelets has been shown to strongly affect Mpl endocytosis associated to MK hyperplasia and myelofibrosis[19]. Deletion of Vps34 in platelets also impacts Mpl and fibrinogen endocytosis but with a somehow different associated phenotype (i.e. moderated microthrombocytopenia without MK hyperplasia) probably due to a different degree of implication of the two proteins in endocytosis and to their impact in other cellular processes.

The α- and dense- granules originate from a multivesicular bodies (MVBs)/late endosome compartment where cargos derive from both a secretory pathway from the golgi network and an endocytic pathway from plasma membrane through highly regulated and still poorly known sorting processes[17,18]. Thus, the aberrant granule biogenesis, highlighted by the disturbed fibrinogen uptake, is consistent with a general trafficking defect of Vps34-deficient MKs and platelets.

PI3P is an important lipid in the regulation of the endocytic pathway and Vps34 has been proposed as the major PI3P producing kinase in mammalian cells[4,5]. Our results show that in MKs, Vps34 controls approximately 40% of the PI3P level, indicating the contribution of other PI3K isoforms in the production of this lipid. Overall our results show that Vps34 controls a PI3P pool important for the regulation of the endocytic and trafficking pathway in MKs. Although we observed a role for Vps34 and PI3P in autophagy in MKs (SS, CV unpublished observation), the trafficking defect shown here appears to be crucial in MK migration and granule biogenesis. This is consistent with the fact that *Pf4*-Cre-*Atg7*$^{lox/lox}$ mice, which exhibit impaired autophagy, have a normal platelet count, size and ultrastructure[38].

Interestingly, in platelets, the contribution of Vps34 to the production of the basal pool of PI3P is very limited (~10%) when compared with the significant contribution of PI3KC2α that we recently described[39]. Several routes of PI3P production probably account for maintaining basal levels of this important lipid, including Vps34 and mainly PI3KC2α but also possibly 4- and/or 5-phosphatses acting on $PI(3,4)P_2$ and/or $PI(3,5)P_2$[40]. However, a significant fraction of the stimulation-dependent PI3P production requires Vps34 activity as shown in platelets from *Pf4*-Cre-*Pik3c3*$^{lox/lox}$ mice and in WT platelets treated in vitro with Vps34 inhibitors. Accordingly, an increase in Vps34 kinase activity was observed following stimulation of WT platelets with G-protein coupled receptors or ITAM-linked receptors. Stimulation-dependent activation of Vps34 has also been suggested in insulin-stimulated hepatocytes[41], pointing towards a role for Vps34 during acute cellular responses.

Acute platelet activation can be triggered in vivo in a thrombosis model of carotid ferric chloride injury. Interestingly, loss of Vps34 in platelets had a significant protective role against occlusive arterial thrombus formation. The decrease in thrombus growth at arterial shear rate was confirmed in ex vivo thrombosis assays using *Pf4*-Cre-*Pik3c3*$^{lox/lox}$ mice blood perfused over a collagen surface and was reproduced by treatment of blood from WT mice or human donors with Vps34 inhibitors, highlighting the important role of Vps34 kinase activity in this process and showing that this effect is not a consequence of Vps34 functions in MKs.

Integrin αIIbβ3 activation and granule secretion are essential for the regulation of thrombus growth[42,43]. The activation of αIIbβ3 integrin appeared not significantly altered in Vps34-deficient platelets and Vps34-deficient washed platelet aggregation in suspension was normal. However, Vps34-deficient platelets showed an increased rate of secretion in response to several agonists in vitro and, importantly, ex vivo under arterial flow. Platelet secretion plays an important physiological role by discharging a variety of molecules contributing to platelet recruitment for adequate thrombus growth and organization. Mathematical models and in vivo

experiments have shown that the architecture of the thrombus (i.e. a stable core of fully-activated, densely-packed platelets with an outer shell of less-activated loosely packed platelets) is the result of overlapping agonist gradients within the platelet mass[33,44,45]. Moreover, a stratified granule secretion has recently been observed in the thrombus with fully degranulated platelets at the base of the thrombus and granule-containing platelets at the vessel lumen[46], demonstrating the importance of secretion events in thrombus formation and organisation. These data indicate that a fine-tuned spatial and temporal regulation of granule release, which is lost in the absence of platelet Vps34 activity, is crucial for normal platelet thrombus formation. Consistent with this, under arterial flow we showed that Vps34-deficient platelets displayed an exacerbated secretion and were less efficient to recruit circulating WT platelets to the growing thrombus. It is not clear at present how Vps34 and its product PI3P contribute to the spatio-temporal platelet secretion but it is most likely due to the recruitment of intracellular proteins that regulate granule fusion and/or secretion.

In conclusion, our study points to a dual function for Vps34 in MKs and platelets. In MKs, Vps34 controls the production of an important pool of PI3P and regulates clathrin-dependent endocytosis and trafficking which in turn impacts on MK migration and the subsequent platelet release in the blood as well as granule biogenesis. In platelets, Vps34 mainly controls the production of a stimulus-dependent pool of PI3P and platelet secretion, thereby impacting on thrombus growth under arterial flow. This study provides new insights into the effects of Vps34 inhibitors in haemostasis and thrombosis that will have to be taken into account if they are used in therapy in the future.

**Acknowledgements**

We thank the personnel of Anexplo animal facilities (US006/CREFRE Inserm/UPS) for animal handling, Genotoul Imaging facilities (INSERM U1048, E. Vega and M. Zanoun; CMEAB, B. Payre and I. Fourqaux), the Cytometry facility of Inserm U1048 (A. Zakaroff-Girard and C. Pecher), and the Lipidomic facility of Inserm U1048 (J. Bertrand-Michel and P. Lefaouder). The authors thank all past and present members from the B.P. laboratory. C.V. was supported by fellowships from Université Toulouse III and Société Francaise d'Hématologie. Work in the laboratory of B.P. was supported by Inserm and Fondation pour la Recherche Médicale (DPC20111122988 to M-P.G. and DEQ20170336737 to B.P.). B.P. is a scholar of the Institut Universitaire de France. Work in the laboratory of B.V. was supported by the Medical Research Council [G0700755], the UK Biotechnology and Biological Sciences Research Council [BB/M013278/1; BB/I007806], Cancer Research UK [C23338/A15965], the Ludwig Institute for Cancer Research and the National Institute for Health Research (NIHR) University College London Hospitals Biomedical Research Centre.

**Authorship Contributions**

C.V., M.L. and S.S. designed research, performed experiments and analyzed data; B.V. and B.B. generated *Pik3c3*$^{lox}$ mice; G.C. and B.P. designed and performed phosphoinositide analysis; C.C. performed arterial thrombosis in vivo; J.V. performed experiments; F.G.I. and M.P.G analyzed data; B.P and S.S. wrote the article.

**Conflicts of Interest Disclosures**

B.V. is consultant to Karus Therapeutics (Oxford, UK).

## REFERENCES


1. Di Paolo G, De Camilli P. Phosphoinositides in cell regulation and membrane dynamics. *Nature*. 2006;443(7112):651-657.

2. Vanhaesebroeck B, Guillermet-Guibert J, Graupera M, Bilanges B. The emerging mechanisms of isoform-specific PI3K signalling. *Nat Rev Mol Cell Biol*;11(5):329-341.

3. Herman PK, Emr SD. Characterization of VPS34, a gene required for vacuolar protein sorting and vacuole segregation in Saccharomyces cerevisiae. *Mol Cell Biol*. 1990;10(12):6742-6754.

4. Schink KO, Raiborg C, Stenmark H. Phosphatidylinositol 3-phosphate, a lipid that regulates membrane dynamics, protein sorting and cell signalling. *Bioessays*. 2013;35(10):900-912.

5. Backer JM. The intricate regulation and complex functions of the Class III phosphoinositide 3-kinase Vps34. *Biochem J*. 2016;473(15):2251-2271.

6. Zhou X, Takatoh J, Wang F. The mammalian class 3 PI3K (PIK3C3) is required for early embryogenesis and cell proliferation. *PLoS One*. 2011;6(1):e16358.

7. Jaber N, Dou Z, Chen JS, et al. Class III PI3K Vps34 plays an essential role in autophagy and in heart and liver function. *Proc Natl Acad Sci U S A*. 2012;109(6):2003-2008.

8. Kimura H, Eguchi S, Sasaki J, et al. Vps34 regulates myofibril proteostasis to prevent hypertrophic cardiomyopathy. *JCI Insight*. 2017;2(1):e89462.

9. Willinger T, Flavell RA. Canonical autophagy dependent on the class III phosphoinositide-3 kinase Vps34 is required for naive T-cell homeostasis. *Proc Natl Acad Sci U S A*. 2012;109(22):8670-8675.

10. Bechtel W, Helmstadter M, Balica J, et al. Vps34 deficiency reveals the importance of endocytosis for podocyte homeostasis. *J Am Soc Nephrol*. 2013;24(5):727-743.

11. Bechtel W, Helmstadter M, Balica J, Hartleben B, Schell C, Huber TB. The class III phosphatidylinositol 3-kinase PIK3C3/VPS34 regulates endocytosis and autophagosome-autolysosome formation in podocytes. *Autophagy*. 2013;9(7):1097-1099.

12. Reifler A, Li X, Archambeau AJ, et al. Conditional knockout of pik3c3 causes a murine muscular dystrophy. *Am J Pathol*. 2014;184(6):1819-1830.

13. Wang L, Budolfson K, Wang F. Pik3c3 deletion in pyramidal neurons results in loss of synapses, extensive gliosis and progressive neurodegeneration. *Neuroscience*. 2011;172:427-442.

14. Zhou X, Wang F. Effects of neuronal PIK3C3/Vps34 deletion on autophagy and beyond. *Autophagy*. 2010;6(6):798-799.

15. Machlus KR, Italiano JE, Jr. The incredible journey: From megakaryocyte development to platelet formation. *J Cell Biol*. 2013;201(6):785-796.

16. Huang Y, Joshi S, Xiang B, et al. Arf6 controls platelet spreading and clot retraction via integrin alphaIIbbeta3 trafficking. *Blood*. 2016;127(11):1459-1467.

17. Ambrosio AL, Boyle JA, Di Pietro SM. Mechanism of platelet dense granule biogenesis: study of cargo transport and function of Rab32 and Rab38 in a model system. *Blood*. 2012;120(19):4072-4081.

18. Blair P, Flaumenhaft R. Platelet alpha-granules: basic biology and clinical correlates. *Blood Rev*. 2009;23(4):177-189.

19. Bender M, Giannini S, Grozovsky R, et al. Dynamin 2-dependent endocytosis is required for normal megakaryocyte development in mice. *Blood.* 2015;125(6):1014-24.

20. Bago R, Malik N, Munson MJ, et al. Characterization of VPS34-IN1, a selective inhibitor of Vps34, reveals that the phosphatidylinositol 3-phosphate-binding SGK3 protein kinase is a downstream target of class III phosphoinositide 3-kinase. *Biochem J*. 2014;463(3):413-427.

21. Ronan B, Flamand O, Vescovi L, et al. A highly potent and selective Vps34 inhibitor alters vesicle trafficking and autophagy. *Nature Chemical Biology*. 2014;10(12):1013-9.

22. Russell RC, Tian Y, Yuan H, et al. ULK1 induces autophagy by phosphorylating Beclin-1 and activating VPS34 lipid kinase. *Nat Cell Biol*. 2013;15(7):741-750.

23. Chicanne G, Severin S, Boscheron C, et al. A novel mass assay to quantify the bioactive lipid PtdIns3P in various biological samples. *Biochem J*. 2012;447(1):17-23.

24. Giuriato S, Pesesse X, Bodin S, et al. SH2-containing inositol 5-phosphatases 1 and 2 in blood platelets: their interactions and roles in the control of phosphatidylinositol 3,4,5-trisphosphate levels. *Biochem J*. 2003;376(Pt 1):199-207.

25. Cataltepe O, Arikan MC, Ghelfi E, et al. Fatty acid binding protein 4 is expressed in distinct endothelial and non-endothelial cell populations in glioblastoma. *Neuropathol Appl Neurobiol*. 2012;38(5):400-410.

26. Rostislavleva K, Soler N, Ohashi Y, et al. Structure and flexibility of the endosomal Vps34 complex reveals the basis of its function on membranes. *Science*. 2015;350(6257):aac7365.

27. Kaushansky K. The molecular mechanisms that control thrombopoiesis. *J Clin Invest*. 2005;115(12):3339-3347.

28. Hattori K, Heissig B, Rafii S. The regulation of hematopoietic stem cell and progenitor mobilization by chemokine SDF-1. *Leuk Lymphoma*. 2003;44(4):575-582.

29. Nilsson SK, Debatis ME, Dooner MS, Madri JA, Quesenberry PJ, Becker PS. Immunofluorescence characterization of key extracellular matrix proteins in murine bone marrow in situ. *J Histochem Cytochem*. 1998;46(3):371-377.

30. Maritzen T, Schachtner H, Legler DF. On the move: endocytic trafficking in cell migration. *Cell Mol Life Sci*. 2015;72(11):2119-2134.

31. Bagaitkar J, Barbu EA, Perez-Zapata LJ, et al. PI(3)P-p40phox binding regulates NADPH oxidase activation in mouse macrophages and magnitude of inflammatory responses in vivo. *J Leukoc Biol*. 2017;101(2):449-457.

32. Stalker TJ, Welsh JD, Tomaiuolo M, et al. A systems approach to hemostasis: 3. Thrombus consolidation regulates intrathrombus solute transport and local thrombin activity. *Blood*. 2014;124(11):1824-1831.

33. Welsh JD, Stalker TJ, Voronov R, et al. A systems approach to hemostasis: 1. The interdependence of thrombus architecture and agonist movements in the gaps between platelets. *Blood*. 2014;124(11):1808-1815.

34. Bender M, Stritt S, Nurden P, et al. Corrigendum: Megakaryocyte-specific Profilin1-deficiency alters microtubule stability and causes a Wiskott-Aldrich syndrome-like platelet defect. *Nat Commun*. 2015;6:6507.

35. Sabri S, Foudi A, Boukour S, et al. Deficiency in the Wiskott-Aldrich protein induces premature proplatelet formation and platelet production in the bone marrow compartment. *Blood*. 2006;108(1):134-140.

36. Dhanjal TS, Pendaries C, Ross EA, et al. A novel role for PECAM-1 in megakaryocytokinesis and recovery of platelet counts in thrombocytopenic mice. *Blood*. 2007;109(10):4237-4244.

37. Paul NR, Jacquemet G, Caswell PT. Endocytic Trafficking of Integrins in Cell Migration. *Curr Biol*. 2015;25(22):R1092-1105.

38. Ouseph MM, Huang Y, Banerjee M, et al. Autophagy is induced upon platelet activation and is essential for hemostasis and thrombosis. *Blood*. 2015;126(10):1224-1233.

39. Valet C, Chicanne G, Severac C, et al. Essential role of class II PI3K-C2alpha in platelet membrane morphology. *Blood*. 2015;126(9):1128-1137.

40. Viaud J, Mansour R, Antkowiak A, et al. Phosphoinositides: Important lipids in the coordination of cell dynamics. *Biochimie*. 2016 Jun;125:250-8.

41. Nemazanyy I, Montagnac G, Russell RC, et al. Class III PI3K regulates organismal glucose homeostasis by providing negative feedback on hepatic insulin signalling. *Nat Commun*. 2015;6:8283.

42. Coller BS, Shattil SJ. The GPIIb/IIIa (integrin alphaIIbbeta3) odyssey: a technology-driven saga of a receptor with twists, turns, and even a bend. *Blood*. 2008;112(8):3011-3025.

43. Golebiewska EM, Poole AW. Platelet secretion: From haemostasis to wound healing and beyond. *Blood Rev*. 2015;29(3):153-162.

44. Leiderman K, Fogelson AL. The influence of hindered transport on the development of platelet thrombi under flow. *Bull Math Biol*. 2013;75(8):1255-1283.

45. Stalker TJ, Welsh JD, Brass LF. Shaping the platelet response to vascular injury. *Curr Opin Hematol*. 2014;21(5):410-417.

46. Eckly A, Rinckel JY, Proamer F, et al. Respective contributions of single and compound granule fusion to secretion by activated platelets. *Blood*. 2016;128(21):2538-2549.

## FIGURE LEGENDS

**Figure 1: Defective platelet production and granule distribution in Vps34-deficient platelets.** (**A**) *Left Panel*, Whole blood platelet count was measured using HORIBA ABX Micros 60 analyzer (mean ± SEM; n=38 mice for WT and 49 for *Pf4*-Cre-*Pik3c3*$^{lox/lox}$ mice (Vps34)); ***p<0.001 versus WT according to two-tailed Student's *t* test). *Middle Panel*, Quantification of the percentage of mice with a mean platelet volume ranging from 4 to 7 µm$^3$ and from 7 to 10 µm$^3$ (mean ± SEM; n=38 mice for WT and 49 for *Pf4*-Cre-*Pik3c3*$^{lox/lox}$ mice (Vps34)). *Right Panel*, Transmission electron microscopy of resting platelets. Images are representative of 5 mice of each genotype. Scale bar: 2 µm. (**B**) Mice were injected intravenously with a dylight$^{488}$-anti-GPIbβ Ig derivative antibody. The percentage of labelled platelets in blood samples was measured at various time points after injection. (**C**) *Left graph*, Thrombocytopenia in mice was induced by intraperitoneal injection of anti-GPIbα antibody. Platelet count was measured in blood samples collected 6 h after injection (time=0) and at various time points. *Middle graph*, Mice serum TPO level was quantified by immunoassay. *Right graph*, Platelets were incubated with 50 ng/mL of TPO at the indicated times and incubated after fixation with a rat antibody against the extracellular domain of Mpl and an anti-rat Alexa Fluor®$^{488}$ antibody. Graph is expressed as percentage of MFI (Mean Fluorescence Intensity) resting (0) values after flow cytometry analysis (mean ± SEM; n=4-6 mice of each genotype, *p<0.05 versus WT according to two-way ANOVA test). (**D**) Transmission electron microscopy of resting platelets. Images are representative of 5 mice of each genotype. Scale bar: 1.5 µm. Arrows indicate α granules. Platelet α- and dense (δ)-granule number and mean area were measured on transmission electron microscopy images using ImageJ (mean ± SEM; n=5 mice of each genotype; *p<0.05, ***p<0.001 versus WT according to two-tailed Student's *t* test).

**Figure 2: Vps34 is critical for MK migration and granule biogenesis.** (**A**) Transmission electron microscopy of MKs from native bone marrow sections. Images are representative of 5 mice of each genotype. Scale bar: 5 µm (upper images) and 1 µm (lower images). α-granule number and mean area were quantified on 70 µm² field of transmission electron microscopy images using ImageJ (mean ± SEM; n=5 mice of each genotype; **p<0.01, ***p<0.001 versus WT according to two-tailed Student's *t* test). (**B**) WT or Vps34-deficient (Vps34) MKs were exposed to a SDF1α gradient within the Dunn chamber. Migration paths over 6 h of 5 representative MKs from 8 independent experiments in each graph were traced. The intersection of the x- and y-axis was taken to be the starting point of each cell path, whereas the source of the SDF1 α was at the top. Accumulated distance and directionality from WT MKs in presence of DMSO (WT) or 1 µM VPS34-IN1 or from Vps34-deficient (Vps34) MKs were analyzed using ImageJ manual tracking plug-in (mean ± SEM; n=30-50 MKs from 8 independent experiments; **p<0.01 versus WT according to one-way ANOVA test). (**C**) Representative confocal images of immunostained native bone marrow. MKs and platelets are labelled by vWF staining (green). FABP4/A-FABP staining (red) labels sinusoid vessels. Nucleus staining was done by DAPI (blue). Scale bars: 50 µm. Graph represents the percentage of platelets inside and outside the sinusoids (mean ± SEM; n= 20 images from 4 mice of each genotype, ***p<0.001 versus WT according to two-tailed Student's *t* test).

**Figure 3: Defective intracellular trafficking and PI3P production in Vps34-deficient MKs.** (**A-C**) MKs uptake of transferrin-Alexa Fluor®$^{546}$ (A) or fibrinogen-Alexa Fluor®$^{488}$ (B-C) was observed by confocal (A) or SIM super resolution microscopy (B-C) at different incubation time points. A-B: Graphs represent fluorescence intensity quantified on a MK *z*-stack by ImageJ or Imaris software. C: Representative three-dimensional surface rendering of

*z*-stacks acquired after 960 min of fibrinogen uptake are shown. Scale bar: 5 µm. Graphs represent fibrinogen-positive structure number and volume quantified over time on three-dimensional images using Imaris software. Data are expressed as mean ± SEM; n=10-60 MKs from 3 mice of each genotype; *p<0.05, ***p<0.001 versus WT according to two-way ANOVA test. (**D**-**E**) Fixed MKs stained with anti-clathrin, anti-EEA1, anti-Rab11 or anti-LAMP1 antibodies followed by corresponding secondary Alexa Fluor®$^{488}$ antibodies were observed by confocal microscopy. Live MKs were stained with LysoTracker® Deep Red, fixed and observed by confocal microscopy. Representative images of a *z*-stack are shown. Scale bar: 5 µm. Graphs represent structure number and area analyzed on a *z*-stack with ImageJ (mean ± SEM; n=30-50 MKs from 3 mice of each genotype; *p<0.05, ***p<0.001 versus WT according to two-tailed Student's *t* test). (**F**) PI3P mass assay performed on MKs as described in methods (mean ± SEM; n=5; **p<0.01 versus WT according one sample *t* test). (**G**) MKs stained with anti-PI3P and secondary Alexa Fluor®$^{488}$ antibodies were observed by confocal microscopy and fluorescence intensity was quantified using ImageJ (mean ± SEM; n=40 MKs from 3 mice of each genotype; ***p<0.001 versus WT according to two-tailed Student's *t* test).

**Figure 4: Vps34 regulates the stimulation-dependent PI3P production in platelets.** (**A**) PI3P content was analysed by mass assay in washed resting WT platelets treated for 1 h with DMSO (WT) or 1 µM VPS34-IN1 and Vps34-deficient platelets (Vps34) (mean ± SEM; n=3-5; **p<0.01 versus WT according to one sample *t* test). (**B**) PI3P content from WT platelets treated for 1 h with DMSO (WT) or 1 µM VPS34-IN1 and from Vps34-deficient platelets (Vps34) in resting or stimulated (CRP, 10 µg/ml; thrombin, 0.5 UI/ml) conditions was assessed by mass assay (mean ± SEM; n=5; *p<0.05; **p<0.01 versus WT according to two-way ANOVA test). (**C**) HPLC analysis of PI3P level of resting and stimulated (CRP, 10

µg/ml; thrombin, 0.5 IU/ml) $^{32}$Pi-labelled platelets (mean ± SD; n=2). (**D**) Vps34 was immunoprecipitated from resting or activated (CRP, 10 µg/ml; thrombin, 0.5 IU/ml) washed platelets and assayed for lipid kinase activity in vitro. Graph represents Vps34 activity (fold increase) normalized to the levels of immunoprecipitated kinase in each condition as assessed by immunoblot and densitometry analysis (mean ± SEM; n=5; ***p<0.001 versus resting according to one sample *t* test).

**Figure 5: Vps34 plays an important role in thrombosis via its kinase activity.** (**A**) Tail bleeding time (n=30 mice of each genotype) was measured as described in methods. (**B**) Thrombotic response of mice to carotid injury after exposure to 7.5 % $FeCl_3$ for 3 min assessed by a flow probe. Graph represents percentage of mice without occlusion 30 min after injury (n=15 mice of each genotype; p=0.0002 according to one sample *t* test). (**C-D**) $DiOC_6$-labelled platelets in mice whole blood were perfused through collagen-coated microcapillaries at a physiological arterial shear rate of 500 $s^{-1}$ (**C**) or at arteriolar shear rate of 1500 $s^{-1}$ (**D**). Scale bar: 20 µm. Surface covered by fluorescent platelets and thrombus volume were analyzed using ImageJ (mean ± SEM; n=8 mice of each genotype; *p<0.05; **p<0.01 versus WT according to two-tailed Student's *t* test and one sample *t* test). (**E**) Healthy human donor whole blood was treated with 1 µM VPS34-IN1, 1 µM SAR405 or vehicle (DMSO) for 1 h. Then, $DiOC_6$-labelled whole blood was perfused through collagen-coated microcapillaries at a physiological shear rate of 1500 $s^{-1}$. Scale bar: 20 µm. Surface covered by fluorescent platelets and thrombus volume were analyzed using ImageJ (mean ± SEM; n=3-5 healthy donors depending on the inhibitor; *p<0.05; **p<0.01 versus vehicle according to two-way ANOVA test and one sample *t* test).

**Figure 6: Vps34 kinase activity regulates platelet secretion.** (**A**) Kinetics of ATP secretion of washed platelets under resting or stimulated conditions (CRP, 1 µg/ml; thrombin, 0.1 IU/ml) were recorded by measuring the luminescence from the firefly luciferin-luciferase reaction by lumi-aggregometry using the Chrono-log aggregometer. Graphs represent percent of WT maximal secretion at 80 sec (mean ± SEM; n=6-15 mice of each genotype depending on the agonist; *p<0.05, **p<0.01 ***p<0.001 versus WT according to two-way ANOVA). (**B**) Kinetics of vWF secretion of washed platelets under resting or CRP (1 µg/ml) or thrombin (0.1 IU/ml) stimulated condition was analyzed by ELISA assay. Results are expressed as fold increase compared to resting WT platelets (mean ± SEM; n=6 mice of each genotype; *p<0.05 versus resting WT according to two-way ANOVA). Kinetics of ATP secretion (**C**) and vWF secretion (**D**) of washed platelets treated 1 h with vehicle (DMSO) or 1 µM VPS34-IN1 and stimulated with CRP (1 µg/ml) or thrombin (0.1 IU/ml) were analyzed as described above (mean ± SEM; n=6; *p<0.05 versus resting WT according to two-way ANOVA). (**E**) Washed platelets were spread on a fibrinogen-coated surface for 20 min in presence or not of apyrase (2 IU/ml) and platelet surface was measured using ImageJ (mean ± SEM; n=3 mice per genotype; **p<0.01 versus WT according to two-way ANOVA). (**F**) Whole blood from WT mice treated for 1 h with DMSO (WT) or 1 µM VPS34-IN1 or from *Pf4*-Cre-*Pik3c3*$^{lox/lox}$ mice was perfused through a collagen-coated microcapillary in presence of fluoxetine (25 µM) at a physiological shear rate of 1500 $s^{-1}$. Serotonin content was quantified in plasma by immunoassay (mean ± SEM normalized by thrombus volume; n=3-5 per condition; ***p<0.001 versus WT according to one-way ANOVA test). (**G**) Unlabelled whole blood from WT or *Pf4*-Cre-*Pik3c3*$^{lox/lox}$ (Vps34) mice were perfused through collagen-coated microcapillaries at 1500 $s^{-1}$ during 1 min and were then replaced by $DiOC_6$-labelled WT whole blood perfused at the same shear rate. Surface covered by fluorescent platelets was

analyzed using ImageJ (mean ± SEM; n=5 mice of each genotype; ***p<0.001 versus WT>WT according to two-way ANOVA test).

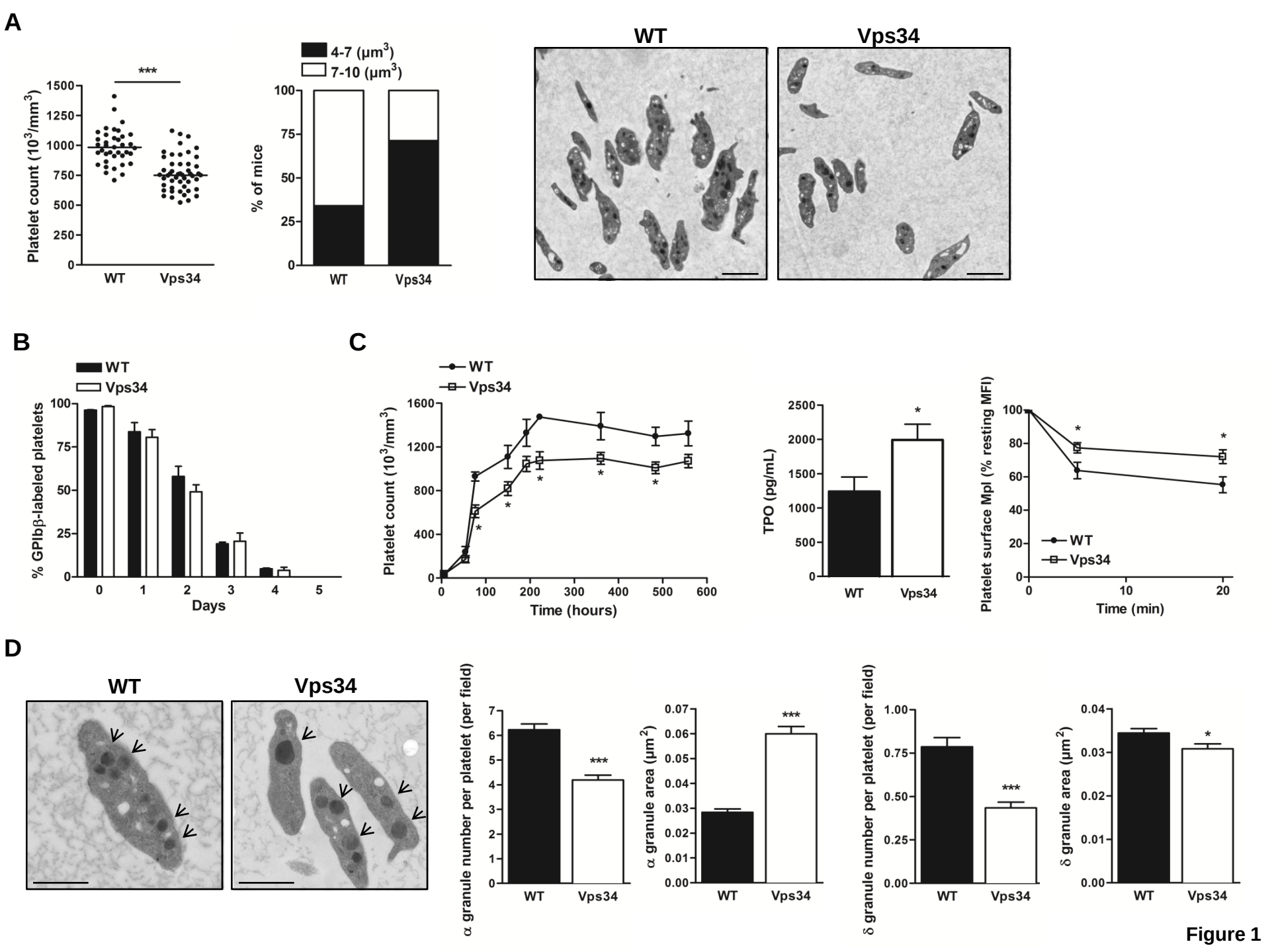
A
Platelet count (10^3/mm^3)
***
WT
Vps34
4-7 (μm^3)
7-10 (μm^3)
% of mice
WT
Vps34
WT
Vps34
B
WT
Vps34
% GPIbβ-labeled platelets
Days
C
WT
Vps34
Platelet count (10^3/mm^3)
Time (hours)
TPO (pg/mL)
WT
Vps34
Platelet surface Mpl (% resting MFI)
WT
Vps34
Time (min)
D
WT
Vps34
α granule number per platelet (per field)
α granule area (μm^2)
δ granule number per platelet (per field)
δ granule area (μm^2)

Figure 1

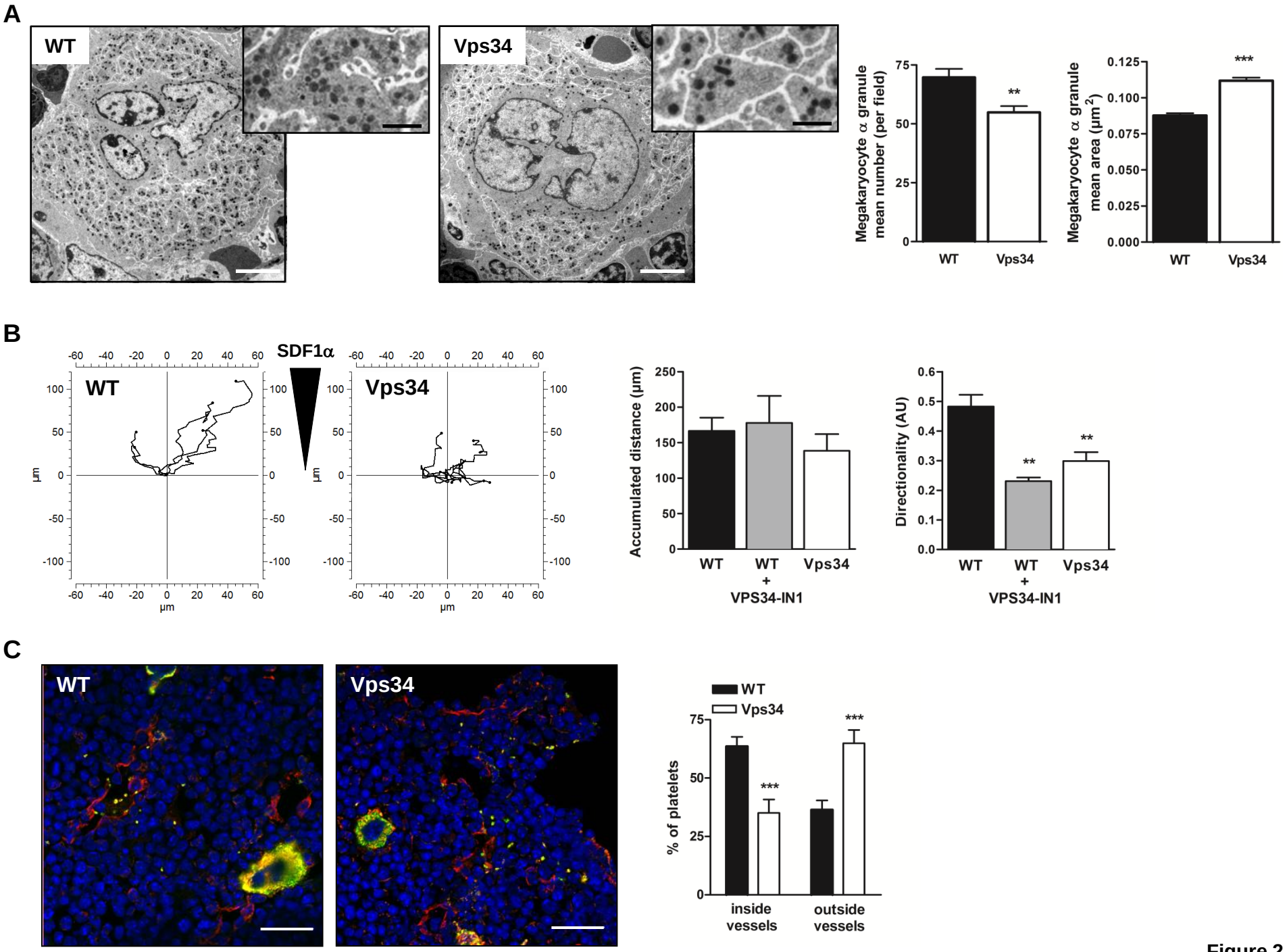
A
WT
Vps34
Megakaryocyte α granule mean number (per field)
Megakaryocyte α granule mean area (μm²)
B
SDF1α
WT
Vps34
μm
Accumulated distance (μm)
Directionality (AU)
WT
WT + VPS34-IN1
Vps34
C
WT
Vps34
% of platelets
inside vessels
outside vessels

Figure 2

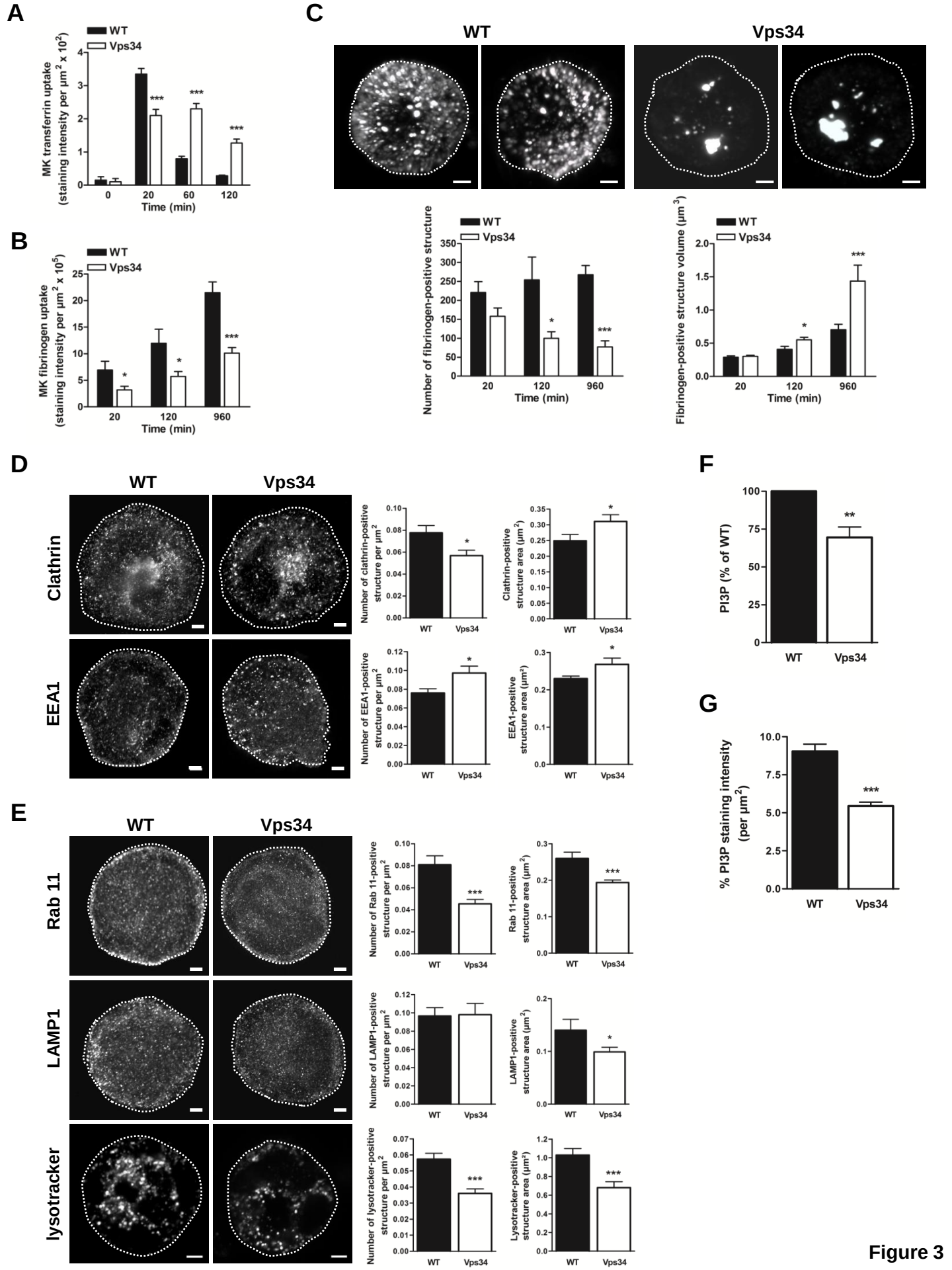
A
WT
Vps34
MK transferrin uptake (staining intensity per µm² x 10²)
Time (min)
B
MK fibrinogen uptake (staining intensity per µm² x 10⁵)
C
WT
Vps34
Number of fibrinogen-positive structure
Fibrinogen-positive structure volume (µm³)
D
Clathrin
EEA1
Number of clathrin-positive structure per µm²
Clathrin-positive structure area (µm²)
Number of EEA1-positive structure per µm²
EEA1-positive structure area (µm²)
E
Rab 11
LAMP1
lysotracker
Number of Rab 11-positive structure per µm²
Rab 11-positive structure area (µm²)
Number of LAMP1-positive structure per µm²
LAMP1-positive structure area (µm²)
Number of lysotracker-positive structure per µm²
Lysotracker-positive structure area (µm²)
F
PI3P (% of WT)
G
% PI3P staining intensity (per µm²)

**Figure 3**

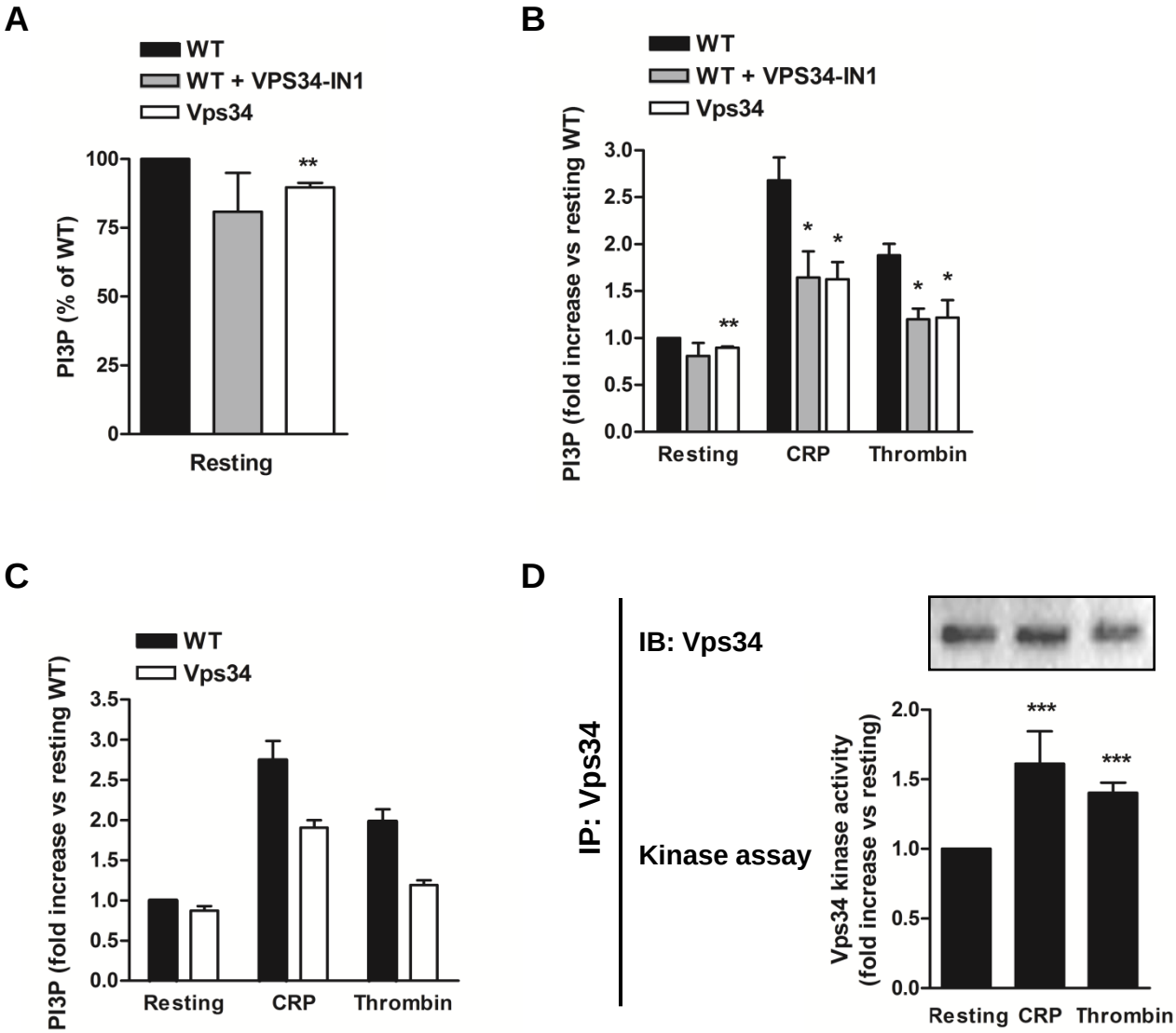
A
WT
WT + VPS34-IN1
Vps34
PI3P (% of WT)
100
75
50
25
0
**
Resting
B
WT
WT + VPS34-IN1
Vps34
PI3P (fold increase vs resting WT)
3.0
2.5
2.0
1.5
1.0
0.5
0.0
**
*
*
*
*
Resting
CRP
Thrombin
C
WT
Vps34
PI3P (fold increase vs resting WT)
3.5
3.0
2.5
2.0
1.5
1.0
0.5
0.0
Resting
CRP
Thrombin
D
IP: Vps34
IB: Vps34
Kinase assay
Vps34 kinase activity
(fold increase vs resting)
2.0
1.5
1.0
0.5
0.0
***
***
Resting
CRP
Thrombin

**Figure 4**

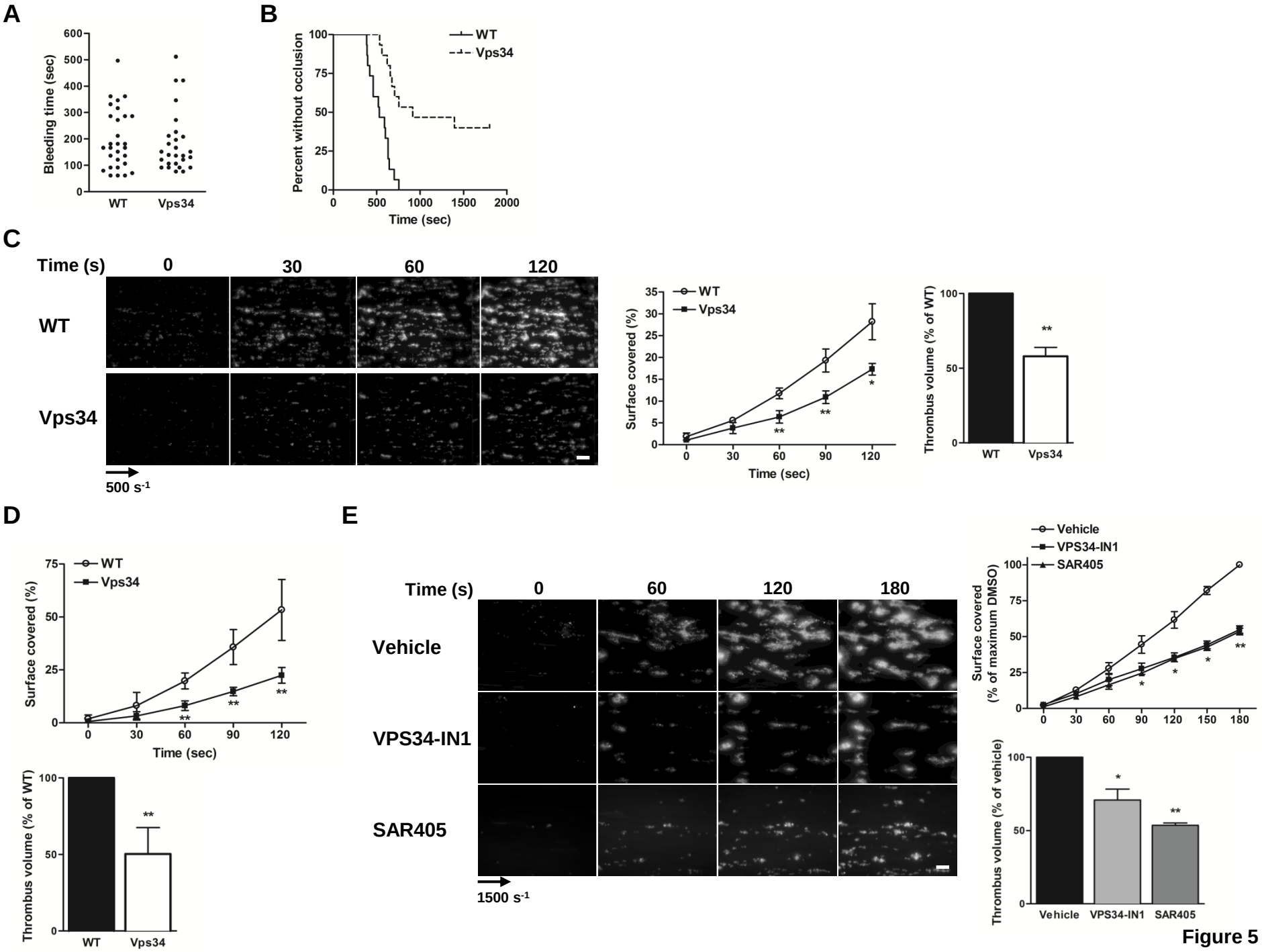
A
Bleeding time (sec)
600
500
400
300
200
100
0
WT
Vps34
B
Percent without occlusion
100
75
50
25
0
0
500
1000
1500
2000
Time (sec)
WT
Vps34
C
Time (s)
0
30
60
120
WT
Vps34
500 s-1
Surface covered (%)
35
30
25
20
15
10
5
0
WT
Vps34
0
30
60
90
120
Time (sec)
Thrombus volume (% of WT)
100
50
0
WT
Vps34
D
Surface covered (%)
75
50
25
0
WT
Vps34
0
30
60
90
120
Time (sec)
Thrombus volume (% of WT)
100
50
0
WT
Vps34
E
Time (s)
0
60
120
180
Vehicle
VPS34-IN1
SAR405
1500 s-1
Vehicle
VPS34-IN1
SAR405
Surface covered (% of maximum DMSO)
100
75
50
25
0
0
30
60
90
120
150
180
Thrombus volume (% of vehicle)
100
50
0
Vehicle
VPS34-IN1
SAR405

Figure 5

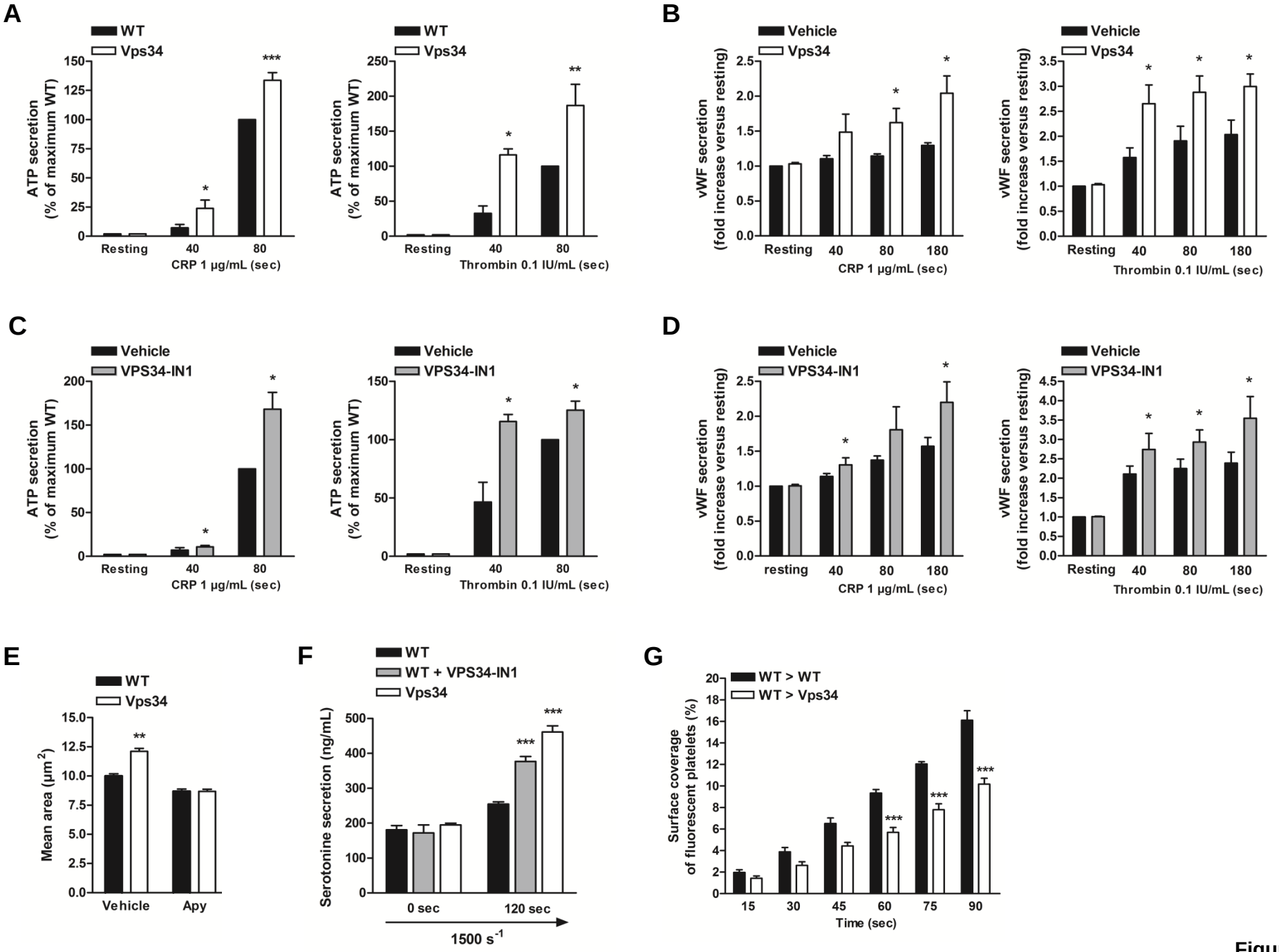
A
WT
Vps34
ATP secretion (% of maximum WT)
Resting
40
80
CRP 1 µg/mL (sec)
Thrombin 0.1 IU/mL (sec)
B
Vehicle
Vps34
vWF secretion (fold increase versus resting)
180
C
VPS34-IN1
D
resting
E
Mean area (µm²)
Vehicle
Apy
F
WT + VPS34-IN1
Serotonine secretion (ng/mL)
0 sec
120 sec
1500 s⁻¹
G
WT > WT
WT > Vps34
Surface coverage of fluorescent platelets (%)
Time (sec)

**Figure 6**

**SUPPLEMENTAL DATA**

## Supplemental Methods

**Materials:** Dylight-anti-GPIbβ Ig derivative, anti-GPIbα-FITC, anti-α2-FITC, JON/A-PE, anti-αIIbβ3-PE, anti-GPVI-FITC and anti-GPIbα (for platelet depletion) antibodies were from Emfret Analytics. Anti-p110α, anti-p110β, anti-hsp90, anti-clathrin and anti-Vps34 (for western blotting) antibodies were purchased from Cell Signaling Technology. Vps34-IN1 was purchased from Medkoo Biosciences, Inc. Anti-Vps34 antibody for immunoprecipitation and anti-PI3P antibody were from Echelon Biosciences Inc. Anti-Vps15 antibody was from Bethyl Laboratories Inc. Anti-p85 antibody was from Merck Millipore. Anti-FABP4/A-FABP antibody and Mouse Thrombopoietin Immunoassay were from RnDSystems. Serotonin ELISA test and anti-Mpl antibody against the extracellular domain were from IBL International. Anti-Mpl antibody for western-blotting was from Novus Biologicals™. Anti-human von Willebrand factor, anti-human von Willebrand factor HRP and anti-human fibrinogen antibodies were purchased from Dako. Lysotracker® Deep Red, MitoTracker® Deep Red$^{FM}$, MitoSOX™ Red mitochondrial superoxide indicator, transferrin-Alexa Fluor®$^{546}$, fibrinogen-Alexa Fluor®$^{488}$ and propidium iodide were obtained from Molecular Probes™. Biochips with microcapillaries (Vena8Fluoro+) were obtained from Cellix. Biotin-conjugated rat anti-mouse CD45R/B220, purified rat anti-mouse CD16/CD32, anti-β1-FITC, anti-GPIIb-FITC, anti-EEA1, anti-LAMP1, anti-PI3KC2α and anti-PI3KC2β antibodies were from BD Pharmingen. Anti-Rab5 and anti-Rab7 antibodies were a gift from F. Alpy (IGBMC, Illkirch, France). Anti-mouse Gr1 and biotin anti-mouse CD11b antibodies were from eBioscience. Anti-Rab11 antibody, sheep anti-rat IgG Dynabeads and StemPro medium were from Invitrogen™. Lipids were from Avanti Polar Lipids (Coger, Paris, France). CRP was

from Pr. R. Farndale laboratory (Cambridge, UK). Collagen Reagent HORM® (equine) suspension was purchased from Takeda. $DIOC_6$ and Alexa Fluor®$^{488}$ anti-mouse / rabbit or rat secondary antibodies were from Life Technologies. Recombinant murine TPO, SCF and SDF1α were obtained from Peprotech. All other reagents were purchased from Sigma-Aldrich.

**MK purification and culture:** Bone marrow cells were obtained from mouse femora and tibiae. Cells expressing one or more of the following surface proteins, CD16/CD32$^+$, Gr1$^+$, B220$^+$, CD11b$^+$, were depleted using immunomagnetic beads (sheep anti-rat IgG Dynabeads). The remaining population was cultured in 2.6% serum-supplemented StemPro medium with 2 mM L-glutamine, penicillin (100 IU/mL)/streptomycin (100 µg/mL), 20 ng/mL murine stem cell factor (SCF) and 50 ng/mL murine thrombopoietin (TPO) at 37°C under 5% $CO_2$ for 3 days. Mature MKs were isolated using a 1.5%-3% bovine serum albumin (BSA) gradient under gravity for 45 min at room temperature.

**Washed murine platelets** were prepared as previously described[1].

**Gel electrophoresis and immunoblotting:** MKs or washed platelets were lysed in Laemmli electrophoresis sample buffer containing 100 mM Tris-HCl (pH 6.8), 15% (v/v) glycerol, 25 mM DTT and 3% SDS, boiled for 5 min, separated on SDS-PAGE, transferred onto a nitrocellulose membrane (Gelman Sciences) and analyzed using the relevant antibody.

**Scanning and Transmission electron microscopy** were performed on washed platelets and freshly isolated bone marrow from tibiae as previously described[1].

**ELISA assays:** Serotonin content was measured using IBL Serotonin ELISA test (RE59121, IBL) according to the manufacturer instructions. Serum TPO quantification was performed using RnDSystems Mouse Thrombopoietin Immunoassay (MTP00, RnDSystems) according

to manufacturer instructions. VWF levels were quantified by a previously described immunosorbent assay[2].

**Flow cytometry:** For surface glycoprotein expression, platelets in whole blood or MKs were stained with anti-α2-FITC, anti-GPVI-FITC, dylight-488-anti-GPIbβ Ig derivative, anti-GPIbα-FITC, anti-β1-FITC, anti-GPIIb or anti-αIIbβ3-PE antibodies for 30 min at room temperature. For Mpl surface expression, washed platelets before or after TPO internalization were fixed with 1.5% formaldehyde for 20 min and incubated with a specific antibody directed against the extra-cellular domain of Mpl followed by a secondary Alexa Fluor®$^{488}$ for 2 h. For mitochondria content, washed platelets were incubated with a specific mitochondria fluorescent-probe (MitoTracker® Deep Red$^{FM}$ and MitoSOX$^{TM}$ Red mitochondrial superoxide indicator) for 30 min at 37°C. For ROS content, washed platelets were incubated with Dichloro-dihydro-fluorescein diacetate (DCFH-DA) for 30 min at 37°C. MK polyploidy was analyzed after MK fixation with 0.5% formalin and subsequent DNA staining with propidium iodide. Samples were analyzed using an LSRFortessa$^{TM}$ Cell analyser flow cytometer and Diva software (Becton Dickinson).

**Immunofluorescence:** MKs were allowed to adhere on a fibronectin-coated surface (20 µg/mL) for 3 h at 37°C. For clathrin, EEA1, Rab11 and LAMP1 staining, MKs were fixed and permeabilized in one step with 3.7% formaldehyde and 0.05% Triton X100 for 45 min. Samples were saturated in 3% fatty acid free BSA for 20 min and incubated with primary antibody and the relevant Alexa Fluor®$^{488}$ secondary antibody for 2 h at room temperature. PI3P labeling using specific anti-PI3P antibody was performed as previously described[3]. For lysosome content analysis, MKs were stained with LysoTracker® Deep Red (100 nM) for 30 min, washed and fixed with 3.7% formaldehyde for 30 min. For endocytosis assays, MKs were incubated for 20 min at 4°C with 20 µg/mL transferrin-Alexa Fluor®$^{546}$ or 200 µM

fibrinogen-Alexa Fluor®$^{488}$, washed and incubated for different times at 37°C before being fixed with 3.7% formaldehyde for 30 min. Confocal images were captured with a LSM780 operated with Zen software using a 63x, 1.4 NA Plan Apochromatic objective lens (Carl Zeiss). SIM (Structured Illumination Microscopy) super-resolution was performed with an ELYRA.PS1 operated with Zen software (Carl Zeiss), using a 63x, 1.4 NA Plan-Apochromat lens and three rotations of a 51-µm grid. Images were captured with a sCMOS camera (Hamamatsu). Image analysis was processed with ImageJ or Imaris software.

**Proplatelet formation assay from bone marrow explants** was performed as previously described[4].

**Platelet lifespan:** Circulating platelets were labelled in vivo by intravenous injection of Dylight$^{488}$-anti-GPIbβ Ig derivative (0.1 µg/g body weight). 2 h after antibody injection and every 24 h for 5 days, the percentage of the Dylight$^{488}$-positive platelet population in whole blood from tail bleeding was determined using an LSRFortessa$^{TM}$ Cell analyser flow cytometer and Diva software (BD Biosciences).

**Immune-induced thrombocytopenia:** Thrombocytopenia was induced by intraperitoneal injection of anti-mouse GPIbα antibody (2 µg/g body weight). Blood samples were collected by tail bleeding at different times and platelet counts were measured using HORIBA ABX Micros 60 analyser.

**Platelet aggregation and dense granule secretion:** Aggregation and adenosine triphosphate (ATP) secretion were measured simultaneously under continuous stirring at 1000 rpm at 37°C using a Born lumi-aggregometer (Chrono-Log).

**αIIbβ3 integrin function assays:** For integrin activation, washed platelets ($1 \times 10^6$) were stimulated with agonists at 37°C for 15 min in presence of 1 mM $Ca^{2+}$ and incubated

subsequently with PE-conjugated JON/A antibody for 30 min at room temperature before being analyzed using an LSRFortessa$^{TM}$ Cell analyser flow cytometer and Diva software (Becton Dickinson). For spreading experiments, washed platelets ($1 \times 10^7$) were allowed to adhere and spread on fibrinogen coated-surface (100 µg/ml) for 20 min at 37°C. Platelets were fixed with 1.5% formaldehyde for 30 min, permeabilised with 0.1% Triton X100 for 10 min and labelled with phalloidin Alexa Fluor®$^{488}$. For endocytosis assays, platelets were incubated for different time points at 37°C with 30 µg/ml fibrinogen-Alexa Fluor®$^{488}$ before being fixed with 1.5% formaldehyde for 30 min. Confocal images were captured with a LSM780 operated with Zen software using a 63x, 1.4 NA Plan Apochromatic objective lens (Carl Zeiss). Image analysis was performed using ImageJ.

**Flow assay on collagen, carotid artery thrombosis and tail bleeding time** were performed as previously described[1,5]. For platelet incorporation assay into an existing thrombus, unlabelled whole blood was perfused through a collagen-coated microcapillary at 1500 $s^{-1}$. After 1 min of flow, blood was replaced by $DiOC_6$-labelled whole blood and perfused for 1 min 30 at 1500 $s^{-1}$. The surface covered (%) by fluorescent platelets was then analyzed using ImageJ.

**TXB2** were analyzed by mass spectrometry as described previously[6].

## References


1. Valet C, Chicanne G, Severac C, et al. Essential role of class II PI3K-C2alpha in platelet membrane morphology. *Blood*. 2015;126(9):1128-1137.

2. Romijn RA, Westein E, Bouma B, et al. Mapping the collagen-binding site in the von Willebrand factor-A3 domain. *J Biol Chem*. 2003;278(17):15035-15039.

3. Posor Y, Eichhorn-Gruenig M, Puchkov D, et al. Spatiotemporal control of endocytosis by phosphatidylinositol-3,4-bisphosphate. *Nature*. 2013;499(7457):233-237.

4. Antkowiak A, Viaud J, Severin S, et al. Cdc42-dependent F-actin dynamics drive structuration of the demarcation membrane system in megakaryocytes. *J Thromb Haemost*. 2016;14(6):1268-1284.

5. Laurent PA, Severin S, Hechler B, Vanhaesebroeck B, Payrastre B, Gratacap MP. Platelet PI3Kbeta and GSK3 regulate thrombus stability at a high shear rate. *Blood*. 2015;125(5):881-888.

6. Le Faouder P, Baillif V, Spreadbury I, et al. LC-MS/MS method for rapid and concomitant quantification of pro-inflammatory and pro-resolving polyunsaturated fatty acid metabolites. *J Chromatogr B Analyt Technol Biomed Life Sci*. 2013;932:123-133.

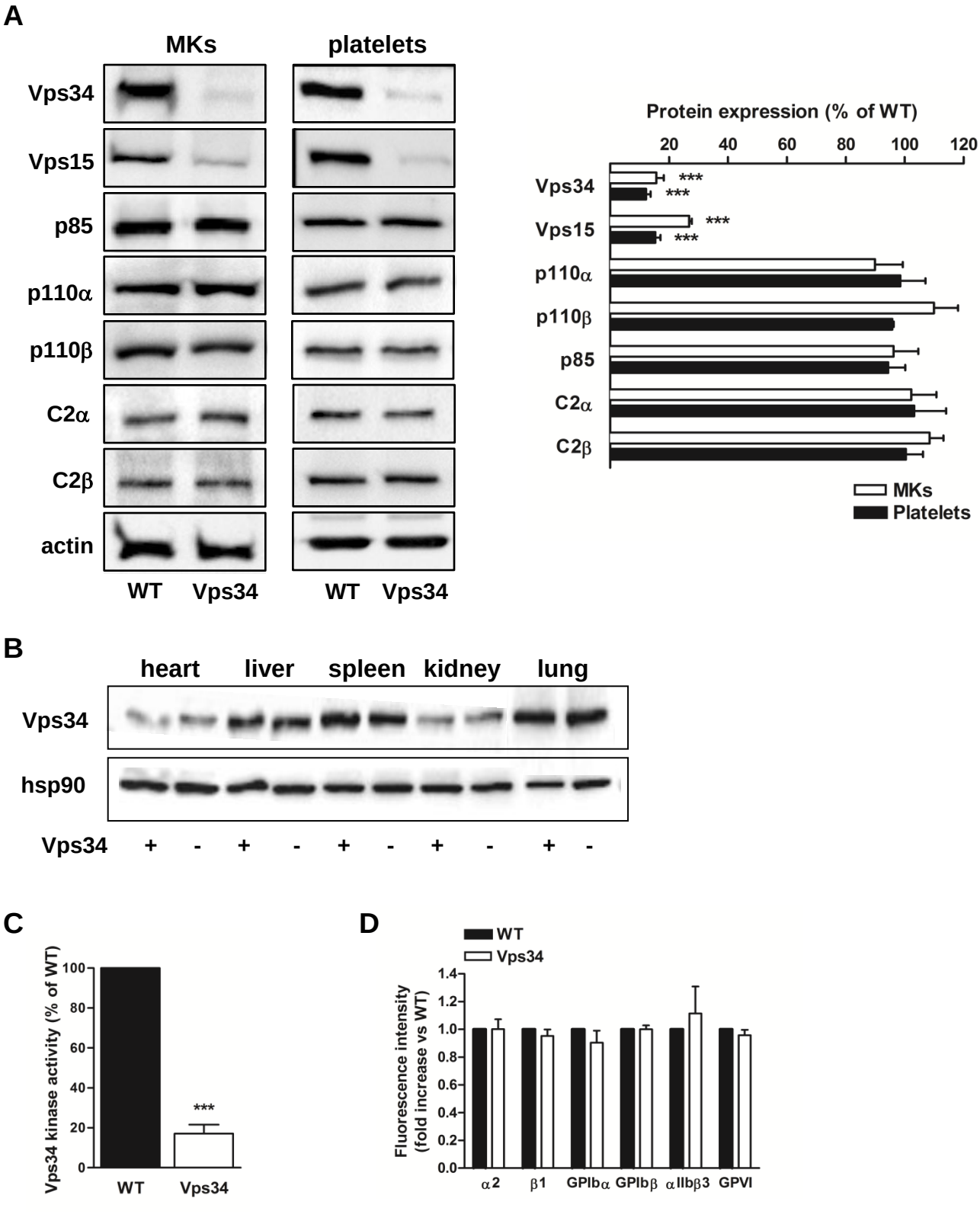


**Figure S1: Conditional genetic inactivation of Vps34 in the MK/platelet lineage**. (**A**) Western blot analysis for Vps34, Vps15, p110α, p110β, p85, PI3KC2α and PI3KC2β in platelet and MK lysates (mean ± SEM; n=3-6; ***p<0.001 versus WT according one sample *t* test). Actin represents the loading control. (**B**) Representative western blot for Vps34 expression in heart, liver, spleen, kidney and lung lysates. Hsp90 represents the loading control. (**C**) Vps34 was immunoprecipitated from resting washed platelets and assayed for lipid kinase activity in vitro (mean ± SEM; n=5; ***p<0.001 versus WT according to one sample *t* test). (**D**) Surface glycoprotein and integrin expression was assessed on resting platelets by flow cytometry (mean ± SEM; n=4).

**Supplemental Figure 1**

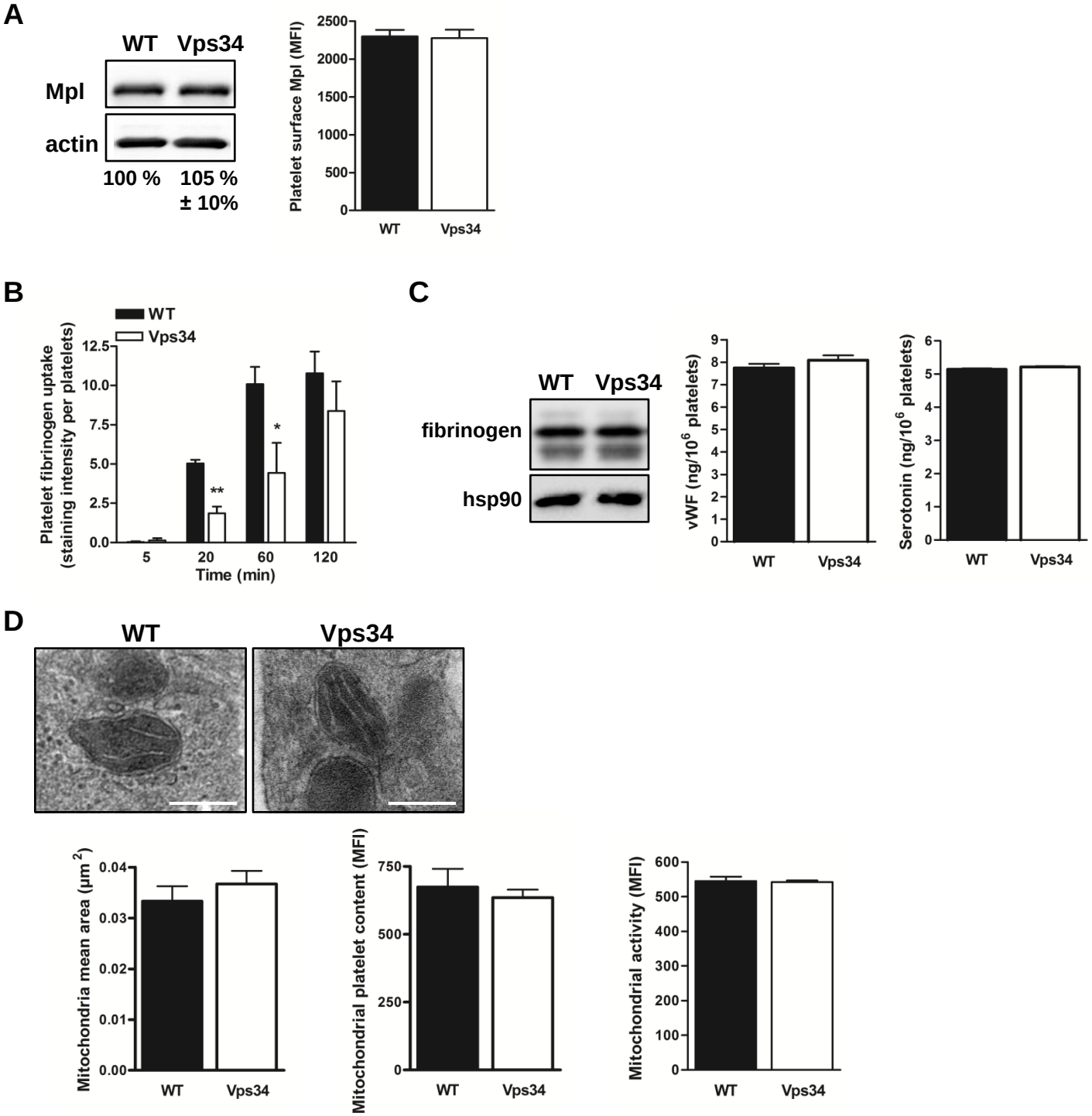


**Figure S2: Normal Mpl expression, granule content and mitochondria in Vps34-deficient platelets.** (**A**) Total and surface expression of Mpl were analyzed by western blot and flow cytometry respectively. Actin is used as loading control. MFI: mean intensity fluorescence (mean ± SEM; n=3-6 mice of each genotype). (**B**) Platelets were incubated with fibrinogen-Alexa Fluor®$^{488}$ and its internalisation was observed by confocal microscopy at different incubation times. Graph represents fluorescence intensity per platelets quantified using ImageJ (mean ± SEM; n=100 platelets from 3 mice of each genotype; *p<0.05, **p<0.01 versus WT according to two-way ANOVA test). (**C**) Platelet vWF, fibrinogen and serotonin global content were quantified by immunoassay or western blot (mean ± SEM; n=6 mice of each genotype). (**D**) Transmission electron microscopy images of platelet mitochondria representative from 3 mice of each genotype. Scale bar: 200 nm. Mitochondria area was quantified using ImageJ (mean ± SEM; n=3 mice/genotype). Platelet mitochondrial content and activity were assessed by flow cytometry using MitoTracker® Red$^{FM}$ and MitoSOX$^{TM}$ Red mitochondrial superoxide indicator staining respectively (mean ± SEM; n=3).

**Supplemental Figure 2**

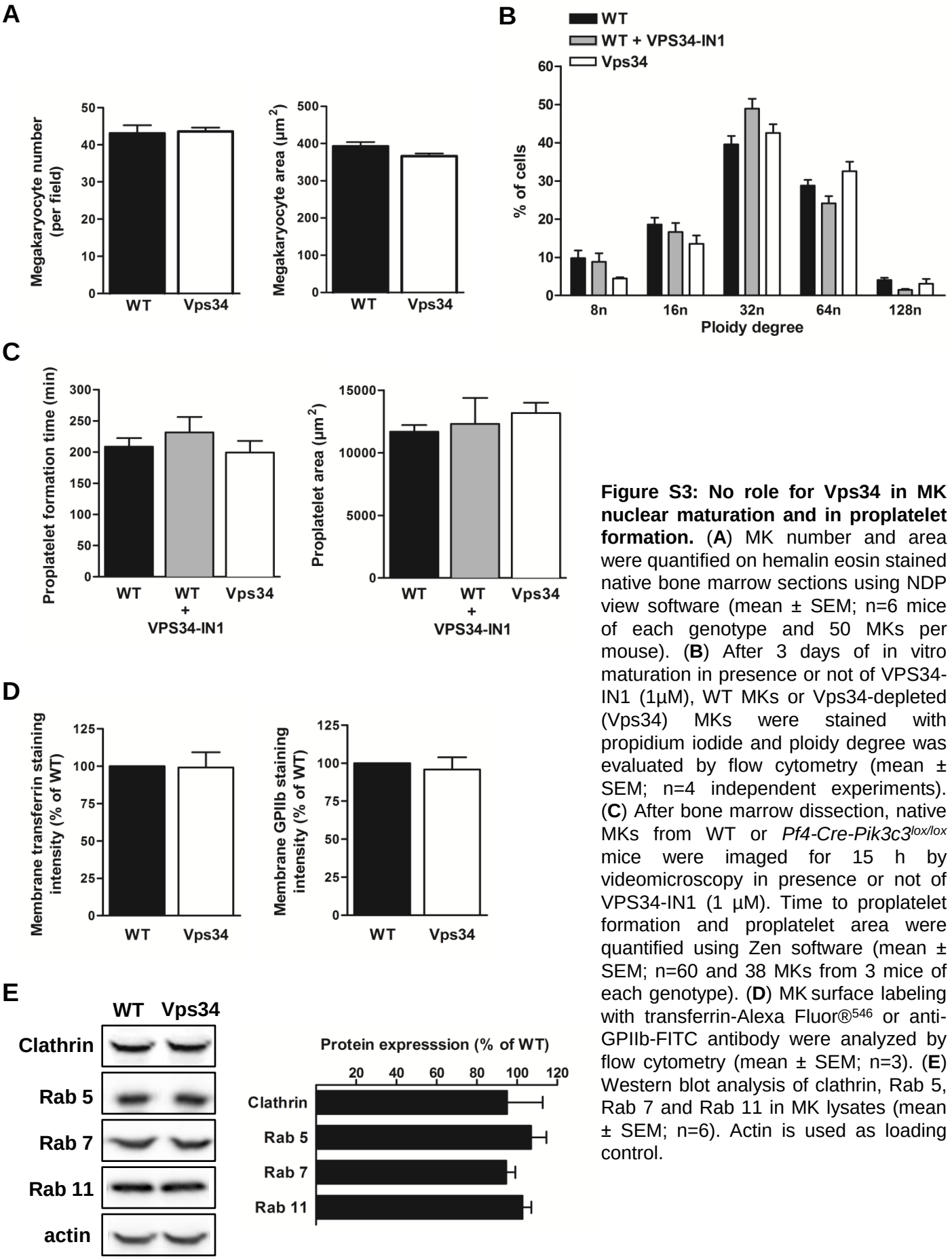


**Figure S3: No role for Vps34 in MK nuclear maturation and in proplatelet formation.** (**A**) MK number and area were quantified on hemalin eosin stained native bone marrow sections using NDP view software (mean ± SEM; n=6 mice of each genotype and 50 MKs per mouse). (**B**) After 3 days of in vitro maturation in presence or not of VPS34-IN1 (1µM), WT MKs or Vps34-depleted (Vps34) MKs were stained with propidium iodide and ploidy degree was evaluated by flow cytometry (mean ± SEM; n=4 independent experiments). (**C**) After bone marrow dissection, native MKs from WT or *Pf4-Cre-Pik3c3*$^{lox/lox}$ mice were imaged for 15 h by videomicroscopy in presence or not of VPS34-IN1 (1 µM). Time to proplatelet formation and proplatelet area were quantified using Zen software (mean ± SEM; n=60 and 38 MKs from 3 mice of each genotype). (**D**) MK surface labeling with transferrin-Alexa Fluor®$^{546}$ or anti-GPIIb-FITC antibody were analyzed by flow cytometry (mean ± SEM; n=3). (**E**) Western blot analysis of clathrin, Rab 5, Rab 7 and Rab 11 in MK lysates (mean ± SEM; n=6). Actin is used as loading control.

**Supplemental Figure 3**

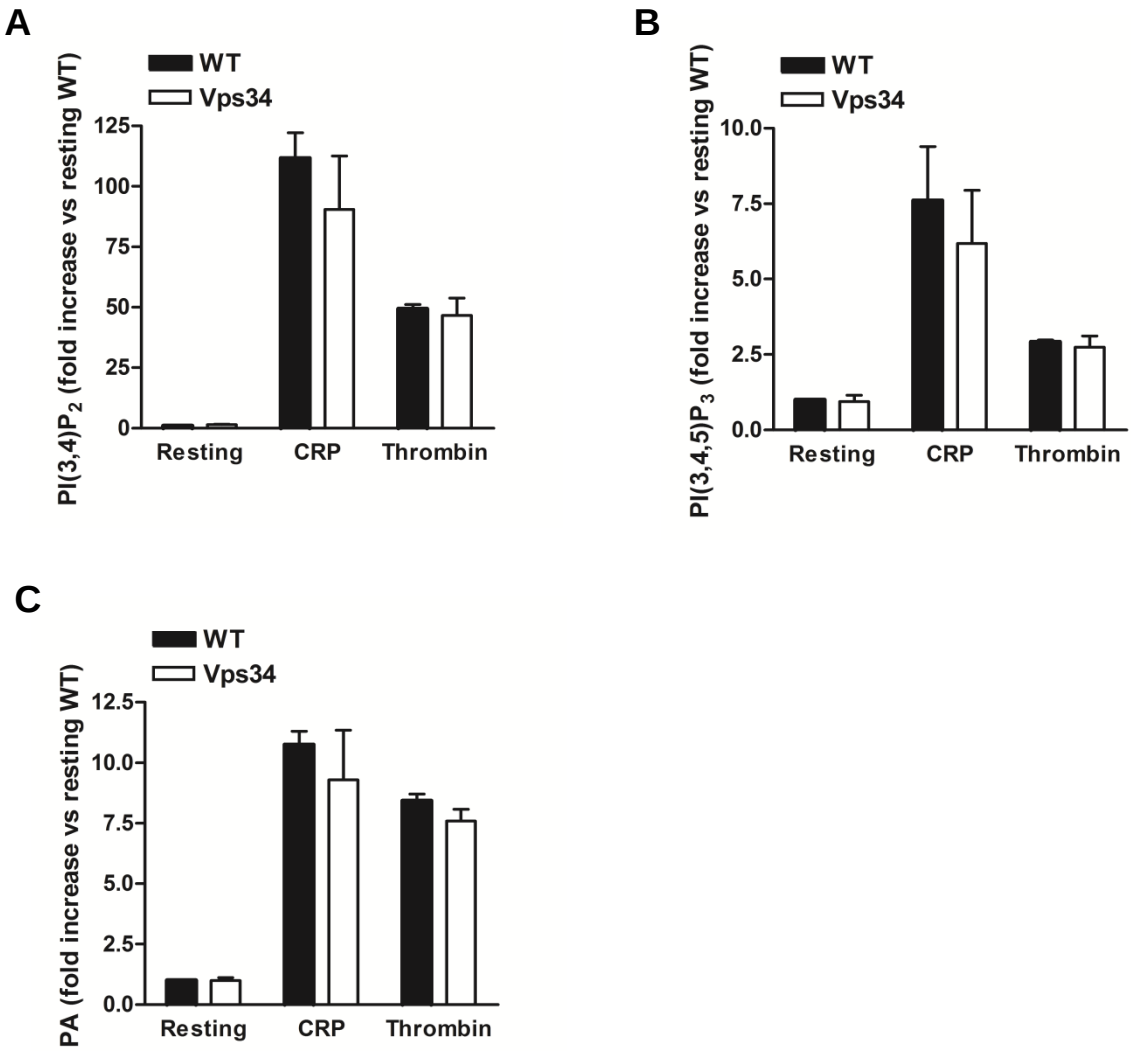


**Figure S4: Normal basal and inducible PI(3,4)$P_2$, PI(3,4,5)$P_3$ and phosphatidic acid levels in platelets.** HPLC analysis of PI(3,4)$P_2$ (**A**) and PI(3,4,5)$P_3$ (**B**) and phosphatidic acid (PA) (**C**) of rested and stimulated (CRP, 10 µg/ml ; thrombin, 0.5 IU/ml) $^{32}$Pi-labelled platelets (mean ± SD; n=2).

**A**

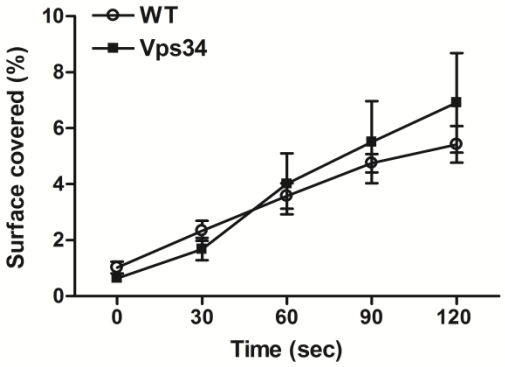


**B**

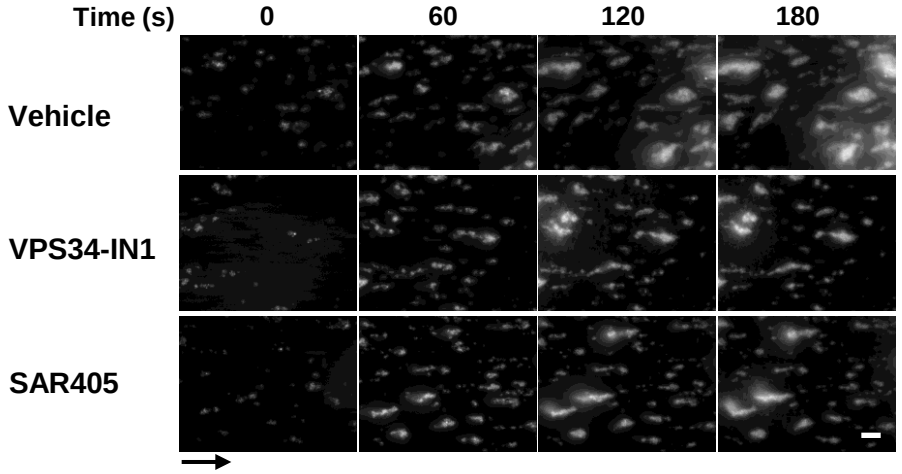


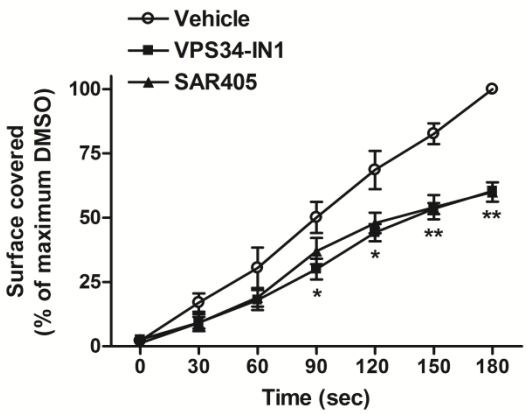


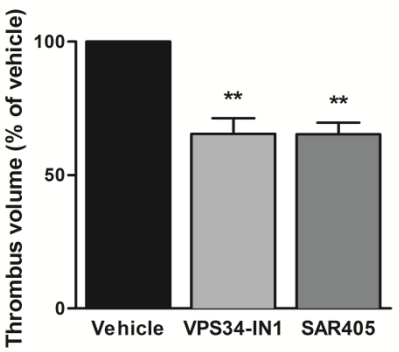


**Figure S5: Vps34 inactivation decreased thrombus growth.** (**A**) Platelet adhesion on collagen surface after αIIbβ3 integrin blockade. $DiOC_6$-labelled platelets in whole blood treated with Integrilin® (40 µg/ml) were perfused through a collagen-coated microcapillary at a physiological shear rate of 1500 $s^{-1}$. Surface covered by fluorescent platelets was analyzed using ImageJ (mean ± SEM; n=3-5 mice of each phenotype). (**B**) Whole blood from WT mice was treated with VPS34-IN1 (1µM), SAR405 (1µM) or vehicle (DMSO) for 1 h. Then, $DiOC_6$-labelled whole blood was perfused through a collagen-coated microcapillary at a physiological arterial shear rate of 500 $s^{-1}$. Scale bar: 20 µm. Surface covered by fluorescent platelets and thrombus volume were analyzed using ImageJ (mean ± SEM; n=5 mice of each genotype; *p<0.05; **p<0.01 versus WT according to two-way ANOVA test and one sample *t* test).

**Supplemental Figure 5**

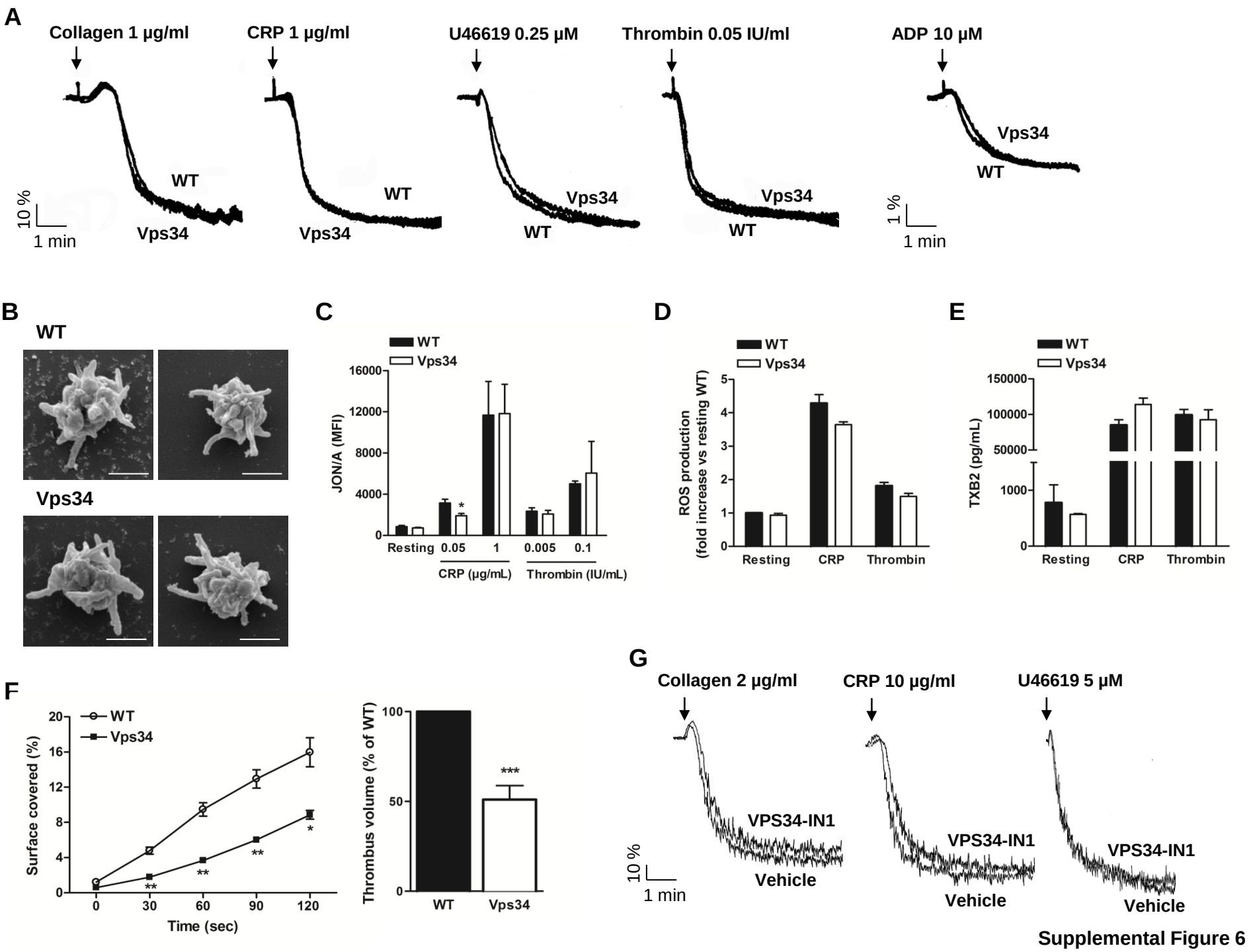


Supplemental Figure 6

**Figure S6: Normal *in vitro* platelet aggregation when Vps34 is deleted or inactivated.** (**A**) Washed platelet aggregation in response to collagen, CRP, thrombin or U46619 or in response to ADP was analyzed by light transmission aggregometry or by impedance aggregometry respectively. Representative curves are shown (n=6-15 mice of each genotype) (**B**) Washed platelets stimulated in suspension with CRP (1 µg/ml) were visualized by scanning electron microscopy. Two representative images of each genotype are representative of 5 mice. Scale bar: 1 µm. (**C**) Flow cytometry analysis of JON/A-PE antibody binding to platelets at resting or stimulated state. Results are cumulative data from 6 mice of each genotype and are presented as mean fluorescence intensity (MFI) ± SEM (*p<0.05 versus WT according to two-way ANOVA). (**D**) Reactive oxygen species (ROS) production in resting or stimulated (CRP, 1 µg/ml; thrombin, 0.1 IU/ml) platelets was analysed by flow cytometry using DCFH-DA compound (mean ± SEM; n=3 mice of each genotype). (**E**) $TXA_2$ production in rested or stimulated (CRP, 1 µg/ml; thrombin, 0.1 IU/ml) platelets was analysed by mass spectrometry by quantifying its stable derivative $TXB_2$ produced (mean ± SEM; n=3 mice of each genotype). (**F**) Platelet adhesion on collagen surface after COX blockade. $DiOC_6$-labeled platelets in indomethacin (10µM) treated whole blood were perfused through a collagen-coated microcapillary at a physiological shear rate of 1500 $s^{-1}$. Surface covered by fluorescent platelets and thrombus volume were analyzed using ImageJ (mean ± SEM; n=3 mice of each phenotype; *p<0.05; **p<0.01; ***p<0.001 versus WT according to two-way ANOVA test and one sample *t* test). (**G**) Platelet-rich plasma from human healthy donors was incubated with DMSO (vehicle) or 1 µM VPS34-IN1 during 1 h at 37°C. Then, platelet aggregation in response to agonists was assessed by light transmission aggregometry. Aggregation curves are representative of 3 healthy donors.

**Video 1 :** WT mice platelet rolling and adhesion on VWF surface. $DiOC_6$-labelled platelets in WT mice whole blood was perfused through a VWF-coated microcapillary at a physiological shear rate of 1500 $s^{-1}$. Transmitted light images were recorded at 0.2 image/sec over the perfusion period using Zen® Zeiss software. Scale bar : 20 µm

**Video 2 :** *Pf4*-Cre-*Pik3c3*$^{lox/lox}$ mice platelet rolling and adhesion on VWF surface. $DiOC_6$-labelled platelets in *Pf4*-Cre-*Pik3c3*$^{lox/lox}$ mice whole blood was perfused through a VWF-coated microcapillary at a physiological shear rate of 1500 $s^{-1}$. Transmitted light images were recorded at 0.2 image/sec over the perfusion period using Zen® Zeiss software. Scale bar : 20 µm